J. Fluid Mech. (2010), *vol.* 660, *pp.* 316–353.
doi:10.1017/S0022112010002788

Weakly nonlinear dynamics of thermoconvective instability involving viscoplastic fluids

C. MÉTIVIER[1]†, C. NOUAR[2] AND J.-P. BRANCHER[2]

[1]Laboratoire de Rhéologie, UMR 5520, Domaine universitaire, BP 53, 38041 Grenoble Cedex, France

[2]LEMTA, UMR 7563, 2 avenue de la forêt de Haye, BP 160, 54504 Vandoeuvre Cedex, France

(Received 30 June 2009; revised 10 May 2010; accepted 12 May 2010;
first published online 4 August 2010)

In this paper, a weakly nonlinear stability of viscoplastic fluid flow is performed. The system consists of a plane Rayleigh–Bénard–Poiseuille (RBP) flow of a Bingham fluid. The basic flow is characterized by a central plug zone, of $2y_b$ width, in which the stresses are smaller than the Bingham number B, the dimensionless yield stress. The Bingham model assumes that inside this zone the material moves as a rigid solid, and that outside this zone it behaves as a viscous fluid. The aim of this study is to investigate the influence of the yield stress on the instability conditions. The linear stability analysis is performed using a modal method and provides critical values of Rayleigh and wavenumbers, from which the system becomes unstable. The critical mode, i.e. the least stable mode, is also determined. This mode, also called the fundamental mode, creates perturbation harmonics which cannot be neglected above criticality. The weakly nonlinear analysis is performed for small-amplitude perturbations. In this study, the quadratic modes of the perturbation are determined. Results indicate that the nonlinear modes perturbation can attain high maximal values, which is the consequence of the high variations of viscosity in the flow. The characterization of the complex Landau equation sheds light on a transition in terms of the bifurcation nature above a critical Péclet number $Pe_c = O(1)$. Below Pe_c, it is found that a supercritical equilibrium state could exist, such as in the Newtonian case, while above Pe_c, the bifurcation becomes subcritical. One observes a sharp transition from supercritical to subcritical bifurcation as the Péclet value is increased. A dependence of Pe_c on the yield stress is highlighted since the subcritical bifurcation is first observed for weak values of y_b ($y_b < O(10^{-1})$). For this range of values, the transition is mainly due to the presence of the unyielded region via non-homogeneous boundary conditions at the yield surfaces. Then for $y_b > O(10^{-1})$, the change of the bifurcation nature is due to the variations of the effective viscosity in the unyielded regions.

Key words: convection, instability, non-Newtonian flows

1. Introduction

We study the stability of the fully developed mixed convection flow, termed the Rayleigh–Bénard–Poiseuille (RBP) flow, for viscoplastic fluids whose rheological behaviour is assumed to be described by the Bingham model (Bingham 1920; Oldroyd 1947*a*, *b*). Even though this model is the simplest one, it accounts for all the features

† Email address for correspondence: christel.metivier@ujf-grenoble.fr

of viscoplastic fluids, namely a yield stress and a shear-thinning behaviour. According to this model, the material moves as a rigid body when the applied stress is less than the yield stress and behaves as a nonlinear viscous fluid above the yield stress.

The RBP flow corresponds to a mixed convection flow between two parallel plates maintained at different temperatures. The RBP flow has two sources of convective instability: the buoyancy-driven source similar to the Rayleigh–Bénard instability (natural convection), which is governed by the Rayleigh number Ra and leads to thermoconvective rolls; the horizontal shear flow governed by the Reynolds number Re which leads at high flow rates to Tollmien–Schlichting waves. The stability of the RBP flow concerns mainly low flow rates. Temporal linear stability analyses were performed by Gage & Reid (1968) for air ($Pr = 1$) and generalized to Newtonian fluids by Platten (1971). These studies show that the Newtonian three-dimensional case can be deduced from the two-dimensional case via the Squire transformation. Moreover, they also show that longitudinal rolls (LRs) (rolls aligned with the shear flow) are less stable than the transversal rolls (TRs) (orthogonal to the shear flow). The LRs are obtained from the critical Rayleigh number $Ra = 1708$ independently from the Reynolds number. Transition from the LRs to TRs is obtained by increasing Ra with an increment proportional to Re^2 for small Reynolds numbers ($Re < O(1)$). Linear stability analysis assumes that the perturbation is small and leads to one unstable mode which is not damped above criticality. Yet, the amplitude perturbation remains locally small since the nonlinear dynamics of the system limits the instabilities increase. Müller, Lücke & Kamps (1989) have studied the nonlinear dynamics of the two-dimensional TRs for weak values of Re. Determining the amplitude evolution via the Ginzburg–Landau equation, the authors highlight a supercritical bifurcation for the Newtonian RBP flow. More recently, the absolute-convective nonlinear stability of the three-dimensional Newtonian RBP flow has been studied when the system is inhomogeneously heated (Carrière & Monkewitz 2001; Martinand, Carrière & Monkewitz 2006). As in the approach of Müller *et al.* (1989), this paper focuses on the weakly nonlinear stability analysis of the two-dimensional Bingham RBP flow for TRs, regardless of their convective or absolute nature. Concerning the shear-thinning and viscoplastic fluids, only a few studies have been performed. Indeed, Khayat (1996), Albaalbaki & Khayat (2008) and Ashrafi & Khayat (1999) investigate the (weakly) shear-thinning effect on the onset of chaos for the two configurations: the Rayleigh–Bénard and the Taylor–Couette. Considering the Carreau–Bird law and deriving the dynamical systems at low order, the authors show that for the two configurations, the shear-thinning precipitates the onset of chaos, via a transition from supercritical to subcritical bifurcation, at a value of control parameter that may be well below the one corresponding to Newtonian fluids. For viscoplastic fluids, a weakly nonlinear analysis has been performed by Cheng & Lai (2008) in the configuration of Bingham vertical-liquid (thin) film which is fully yielded. This paper highlights clearly the change in the nature of the bifurcation as observed by Khayat and co-workers. This transition has also been observed qualitatively by Balmforth & Rust (2009) in the Rayleigh–Bénard configuration. In this paper, approximations are made assuming that the perturbation is strong enough to exceed the yield stress in the whole domain leading to a fully yielded fluid. In these two configurations, the authors do not have to treat the two phases (liquid-like phase and solid-like phase, respectively) of the material. In this paper, we propose to study the weakly nonlinear instability of the Bingham RBP flow dealing with the two phases, which is a major difficulty involved by the viscoplastic fluids. To our knowledge, the weakly nonlinear analysis of viscoplastic fluids dealing directly with the yield stress conditions has never been performed.

The primary flow of the plane Bingham RBP configuration is characterized by a central unyielded region moving at a constant velocity and yielded regions on the both sides. The linear stability of this flow regarding the TRs rolls has been studied by Métivier, Nouar & Brancher (2005) and Métivier & Nouar (2008) via temporal and energetic approaches. In the linear stability analysis, the base flow is subjected to small perturbations for which the amplitude perturbation is not large enough to break up the unyielded region. In other words, the topology is implicitly assumed to be unchanged. Métivier & Nouar (2008) determined the critical conditions above which propagating convective patterns in the form of travelling waves appear on both sides of the plug zone. It is shown that the yield stress has a stabilizing effect via the presence of the unyielded region and the increase in the effective viscosity in the flow domain. These last conclusions are similar for the modal and energetic approaches for small values of Reynolds number, i.e. $Re < O(1)$. However, the numerical results indicate a discrepancy between the critical conditions obtained via the two approaches which is enhanced from $Re > O(1)$ and for increasing Re values. This discrepancy highlights the non-normality of the linear operator which is a necessary condition for a transient growth of the energy perturbation. Métivier *et al.* (2005) investigated the case where the yield stress tends to zero and showed that the critical conditions do not tend to the ones obtained in the Newtonian RBP case since the unyielded region remains intact. In this situation, the problem has to be compared to the Newtonian–Couette RBP stability flow.

Above criticality, the perturbation evolution can be obtained via a weakly nonlinear analysis determining the amplitude equation, in particular in this study, the evolution in time of the perturbation amplitude A. The amplitude equation, i.e. the complex Landau equation, can be written as

$$\partial_t A = \sigma\, A + \lambda_1 |A|^2 A, \tag{1.1}$$

with σ the growth rate determined from the linear theory and λ_1 the first correction regarding the nonlinearities.

As in the linear stability analysis, the framework of the weakly nonlinear analysis corresponds to a small-amplitude perturbation compared with all the scales of the basic flow. As a consequence, the unyielded region is weakly perturbed and the yield surface topology remains similar to the basic state topology, i.e. the yield surfaces separate the flow domain into yielded and unyielded regions, respectively. This consideration is fundamental for our study since it permits us to know *a priori* the structure of the flow.

Once the perturbation becomes finite, the topology of the perturbed flow is unknown *a priori* since the stresses remain indeterminate in the unyielded regions and since the boundaries of such zones are implicitly determined. The nonlinear stability of the plane Bingham RBP flow has been performed by Métivier, Frigaard & Nouar (2009). Using an energetic approach and some approximations on the stress perturbation, the bounds and tendencies for stability conditions as function of the yield stress have been determined.

The aim of this paper is to characterize the influence of the yield stress and the shear-thinning behaviour on the nonlinear features of the perturbed flow by considering a small perturbation. In this respect, a weakly nonlinear stability analysis is performed in order to obtain the complex amplitude equation. The current derivation follows the one developed by Reynolds & Potter (1967) and Herbert (1983), and consists of introducing a double expansion in terms of the Fourier series and linear eigenfunctions in the hydrodynamical and thermodynamical equations.

Fujimura (1989) and Fujimura (1997) showed that the amplitude equation derived by the formal expansion in linear eigenfunctions is equivalent to the one derived by the method of multiple scales. A brief outline of the paper is given as follows. After presenting the basic state of the Bingham RBP flow in § 2, the mathematical formulation of the weakly nonlinear analysis is developed in § 3, treating both the unyielded and yielded regions as well as the non-material interfaces involved by the two phases. This section presents the nonlinear motion and heat equations in both regions as well as the boundary conditions associated with the configuration. Considering the classical form of the perturbation, i.e. a fundamental mode, and the harmonics created from the fundamental mode via the nonlinearities, the motion and heat equations satisfied by the first harmonic (modes 0 and 2) are also developed. This section ends with the formulation of the amplitude equation. The numerical results are presented in § 4. It first recalls briefly the critical conditions, i.e. critical parameters values, critical modes and also the adjoint mode, obtained from the linear stability analysis. Then the section is devoted to presenting the results of the first harmonic and finally the amplitude equation coefficients, allowing us to predict the nature of the bifurcation. New results are presented and thoroughly discussed. Finally, § 5 summarizes the main findings obtained in this study.

2. Base flow

We consider a Bingham-fluid flow in a horizontal plane channel under the action of imposed constant axial pressure gradient. The lower wall is kept at a temperature T_1 higher than that of the upper wall temperature T_2. The non-dimensional velocity, pressure and temperature fields ($\boldsymbol{U}$, P, T) are solutions of the continuity, momentum and energy equations. Considering the Boussinesq approximation, i.e. considering that the fluid-density variation is negligible except in the buoyant effects, they are given by

$$\nabla \cdot \boldsymbol{U} = 0, \tag{2.1a}$$

$$Re\, \boldsymbol{U}_t + Re^2\, Pr\, (\boldsymbol{U} \cdot \nabla)\, \boldsymbol{U} = -Re\, Pr\, \nabla P + Ra\, T\, \boldsymbol{e}_y + Re\, Pr\, \nabla \cdot \boldsymbol{\tau}, \tag{2.1b}$$

$$T_t + Re\, Pr\, (\boldsymbol{U} \cdot \nabla)\, T = \nabla^2 T. \tag{2.1c}$$

The non-dimensional form of the above equations is obtained by using the channel width $\hat{L}$, the diffusion time $\hat{L}^2/\hat{a}$ and the plastic viscosity $\hat{\mu}_0$, as characteristic scales for lengths, time and viscosity, respectively. Here, $\hat{a}$ is the thermal diffusivity. As the basic state is a pressure-driven flow, the maximum of the axial velocity $\hat{U}_0$ is taken as a characteristic scale for the velocities. In the buoyancy-driven problem, the velocity of the thermal diffusion has a key role in the evolution of the perturbation, and therefore has been used as a characteristic scale for the velocities in the stability analysis. The nominal stress $\hat{\mu}_0 \hat{U}_0/\hat{L}$ stands for the stresses and pressure characteristic scales. The temperature difference $\delta \hat{T} = \hat{T}_1 - \hat{T}_2$ provides a reference value for the temperatures: $T = (\hat{T} - \hat{T}_0)/\delta \hat{T}$. The resulting control parameters, the Reynolds, Prandtl and Rayleigh numbers, respectively, are given by

$$Re = \frac{\widehat{\rho} \widehat{U}_0 \widehat{L}}{\widehat{\mu}_0}, \quad Pr = \frac{\widehat{\mu}_0}{\widehat{\rho}\widehat{a}} \quad \text{and} \quad Ra = \frac{\widehat{\rho}\beta g \delta \widehat{T} \widehat{L}^3}{\widehat{\mu}_0 \widehat{a}},$$

where β is the thermal expansion, $\widehat{\rho}$ the material density and $\widehat{g}$ the gravitational acceleration.

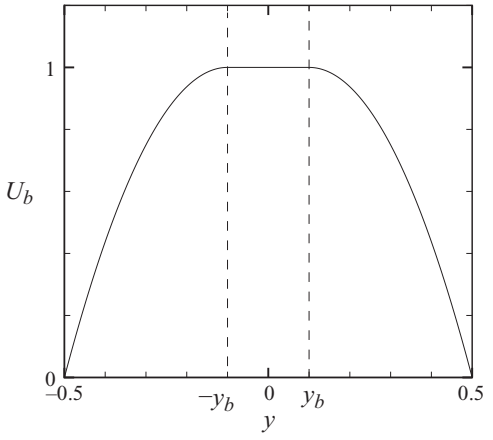

FIGURE 1. Velocity profile for $y_b = 0.1\,(B = 1.25)$. The central plug region is indicated by the dashed lines.

Moreover, $\boldsymbol{\tau}$ is the deviatoric stress tensor determined by the constitutive Bingham model:

$$\boldsymbol{\tau} = \mu \dot{\boldsymbol{\gamma}} \quad \text{if and only if} \quad \tau > B, \tag{2.2a}$$

$$\dot{\gamma} = 0 \quad \text{if and only if} \quad \tau \leqslant B, \tag{2.2b}$$

with $\mu = 1 + (B/\dot{\gamma})$ the effective viscosity, $\dot{\boldsymbol{\gamma}}$ the rate of strain tensor, $\tau = (\tau_{ij}\,\tau_{ij}/2)^{1/2}$ and $\dot{\gamma} = (\dot{\gamma}_{ij}\,\dot{\gamma}_{ij}/2)^{1/2}$ the second invariants of the tensors $\boldsymbol{\tau}$ and $\dot{\boldsymbol{\gamma}}$. The Bingham number is given by $B = \widehat{\tau}_0/(\widehat{\mu}_0\,\widehat{U}_0/\widehat{L})$, where $\widehat{\tau}_0$ is the yield stress. When $\tau \leqslant B$, the material behaves from the kinematic point of view as a rigid solid and the stresses are not determined.

The regions where $\tau \leqslant B$ are termed as unyielded regions or plug zones. They are bounded by yield surfaces defined by the condition $\tau = B$. The motion of these non-material surfaces is determined only by the stress field in the yielded zone.

The steady laminar flow is the plane Bingham–Poiseuille flow with a vertical thermal stratification:

$$U_b(y) = \begin{cases} 1 & \text{for} \quad |y| \leqslant y_b, \\ 1 - \left(\dfrac{|y| - y_b}{1/2 - y_b}\right)^2 & \text{for} \quad y_b < |y| < 1/2, \end{cases} \tag{2.3}$$

$$T_b = -y \tag{2.4}$$

and

$$p_b\,(x, y) \;=\; p_{ref} - Ra\,\frac{y^2}{2} - \frac{2}{((1/2) - y_b)^2}\,x, \tag{2.5}$$

where p_{ref} is a reference pressure.

This fully developed flow is mainly characterized by a central plug zone of $2y_b$ width which moves as a rigid solid (figure 1) and a nonlinear variation of the effective viscosity in the yielded region. According to the Bingham model, μ increases from the wall and tends to infinity near the yield surface, as shown in figure 2, where the viscosity profile is displayed for different values of y_b. In figure 2, one can notice that

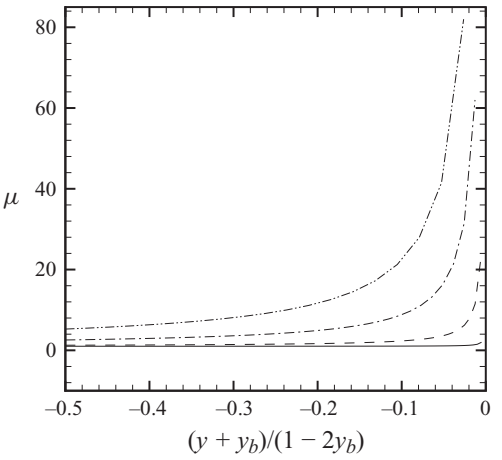

FIGURE 2. Evolution of the effective viscosity in the lower yielded region for different values of y_b: ——— —, $y_b = 0.005$ ($B = 0.04$); - - -, $y_b = 0.105$ ($B = 1.34$); —·—·—, $y_b = 0.305$ ($B = 16.04$); —··—··—, $y_b = 0.405$ ($B = 89.75$).

the higher the yield stress is, the higher the degree of nonlinearity of the rheological behaviour becomes.

The B-dependency of y_b is deduced from the relation $\tau_{xy} = -(\partial P/\partial x)y$, written at the wall, combined with (2.5). One can easily obtain

$$B(1 - 2y_b)^2 - 8y_b = 0, \tag{2.6}$$

which has one physical solution:

$$y_b = \frac{2 + B - 2\sqrt{B+1}}{2B}. \tag{2.7}$$

3. Stability analysis: mathematical formulation

3.1. *Governing equations*

This section is devoted to the weakly nonlinear stability analysis of the basic state defined in the previous section. For that purpose, a perturbation $\boldsymbol{V} = (\psi, \theta)^T$ is added to the basic state $(\psi_b, T_b)^T$, where ψ corresponds to the streamfunction defined by $\partial_x \psi = -v$ and $\partial_y \psi = u$ for the velocity $\boldsymbol{u} = (u, v)^T$; and the exponent T denotes the matrix transposition.

The perturbed flow $(\psi_b + \psi, T_b + \theta)^T$ satisfies the conservation equations. Subtracting out the base-flow equations, the perturbation equations are obtained as

$$\mathscr{D}\frac{\partial \boldsymbol{V}}{\partial t} = \mathscr{L}_R \boldsymbol{V} + \boldsymbol{N}_2(\boldsymbol{V}, \boldsymbol{V}) + \boldsymbol{N}_3(\boldsymbol{V}, \boldsymbol{V}, \boldsymbol{V}) + \cdots, \tag{3.1}$$

where $\mathscr{D}$ is a diagonal matrix, $\mathscr{L}_R$ represents the linear operator and $\boldsymbol{N}_2(\boldsymbol{V}, \boldsymbol{V})$, $\boldsymbol{N}_3(\boldsymbol{V}, \boldsymbol{V}, \boldsymbol{V})$ the quadratic and cubic nonlinear terms, respectively. Here, $\mathscr{D}$ and $\mathscr{L}_R$ are matrices of linear operators:

$$\mathscr{D} = \begin{pmatrix} \mathscr{D}_1 & 0 \\ 0 & \mathscr{D}_2 \end{pmatrix} \tag{3.2}$$

and

$$\mathscr{L}_R = \begin{pmatrix} \mathscr{L}_{R1} & \mathscr{L}_{R2} \\ \mathscr{L}_{R3} & \mathscr{L}_{R4} \end{pmatrix}. \tag{3.3}$$

The quadratic and cubic nonlinear terms may be written in a vectorial form as $\boldsymbol{N}_2(\boldsymbol{V}, \boldsymbol{V}) = (N_{21}, N_{22})^T$ and $\boldsymbol{N}_3(\boldsymbol{V}, \boldsymbol{V}, \boldsymbol{V}) = (N_{31}, N_{32})^T$. The expressions of the different operators are given in the following paragraphs.

At the walls, we write the no-slip conditions and the imposed temperature conditions, respectively, as follows:

$$\partial_y \psi \left(\pm\tfrac{1}{2}\right) = -\partial_x \psi \left(\pm\tfrac{1}{2}\right) = 0, \tag{3.4}$$

$$\theta \left(\pm\tfrac{1}{2}\right) = 0. \tag{3.5}$$

At the yield surfaces, $y = y_i^{\pm}$, the following condition must be satisfied:

$$\dot{\gamma}_{ij} \left(\boldsymbol{U}_b + \boldsymbol{u}\right)|_{y_i^{\pm}} = 0, \tag{3.6}$$

as well as the velocity continuity. Considering that $y_i^{\pm} = \pm y_b \pm Y^{\pm}$, one obtains the following conditions for the yield surfaces:

$$\partial_{xy}\psi|_{\pm y_b} + (\pm Y^{\pm})\partial_{xyy}\psi|_{\pm y_b} + \frac{(\pm Y^{\pm})^2}{2}\partial_{xyyy}\psi|_{\pm y_b} + \cdots = 0, \tag{3.7}$$

$$\partial_y U_b|_{\pm y_b} + (\pm Y^{\pm})\partial_{yy} U_b|_{\pm y_b} + \partial_{yy}\psi|_{\pm y_b} + (\pm Y^{\pm})\partial_{yyy}\psi|_{\pm y_b} + \frac{(\pm Y^{\pm})^2}{2}\partial_{yyyy}\psi|_{\pm y_b} + \cdots = 0 \tag{3.8}$$

and

$$\partial_{xx}\psi|_{\pm y_b} + (\pm Y^{\pm})\partial_{xxy}\psi|_{\pm y_b} + \frac{(\pm Y^{\pm})^2}{2}\partial_{xxyy}\psi|_{\pm y_b} + \cdots = 0. \tag{3.9}$$

Here $\pm Y^{\pm}$ corresponds to the perturbation of the upper yield surface (+) and the lower yield surface (−), respectively. Details of the development of the yield surface conditions are given in Appendix A.

As a remark, one can highlight that in (3.8) the second derivative of U_b is not continuous at $y = \pm y_b$. It implies that this condition has to be considered on both sides of the yield surfaces, i.e. considering the yielded and the unyielded sides separately.

3.2. *Vorticity equation*

According to the Bingham model, we have $\dot{\gamma}_{ij} = 0$ in the unyielded region. Assuming that the perturbation is periodic in the streamwise and spanwise directions, the unyielded region moving as a rigid body can have only a translational motion. Thus, inside the plug, the velocity $\boldsymbol{u}_B$ is independent of the spatial coordinates:

$$\boldsymbol{u} = \boldsymbol{u}_B(t), \tag{3.10}$$

in other words,

$$\partial_x \boldsymbol{u} = \partial_y \boldsymbol{u} = \boldsymbol{0}. \tag{3.11}$$

In the yielded regions, i.e. regions where $\tau > B$, the deviatoric stress tensor for the perturbed flow is expanded about the base flow as

$$\tau_{ij} = \tau_{bij} + \tau'_{ij}, \tag{3.12}$$

where $\boldsymbol{\tau}' = \sum_{k=1}^{N} \boldsymbol{\tau}_k + O((\dot{\gamma}')^{N+1})$ is the stress tensor perturbation, and

$$\tau_{1ij} = \left.\frac{\partial \tau_{ij}}{\partial \dot{\gamma}_{kl}}\right|_b \dot{\gamma}'_{kl}, \tag{3.13}$$

$$\tau_{2ij} = \frac{1}{2}\left.\frac{\partial^2 \tau_{ij}}{\partial \dot{\gamma}_{kl}\partial \dot{\gamma}_{mn}}\right|_b \dot{\gamma}'_{kl}\dot{\gamma}'_{mn}, \tag{3.14}$$

$$\tau_{3ij} = \frac{1}{6}\left.\frac{\partial^3 \tau_{ij}}{\partial \dot{\gamma}_{kl}\partial \dot{\gamma}_{mn}\partial \dot{\gamma}_{pq}}\right|_b \dot{\gamma}'_{kl}\dot{\gamma}'_{mn}\dot{\gamma}'_{pq}. \tag{3.15}$$

The index b means that the terms are evaluated at $\boldsymbol{U}_b$, the base flow. One can notice that $\boldsymbol{\tau}_1$, $\boldsymbol{\tau}_2$, $\boldsymbol{\tau}_3$ correspond, respectively, to the linear, bilinear and trilinear stress tensor perturbation since the only perturbation terms spring from the $\dot{\gamma}'$ components.

Since the problem considered is bidimensional, defining $\dot{\gamma}^b = |\dot{\gamma}_{xy}(\boldsymbol{U}_b)| = |\partial_y U_b|$ and $\tau_b = \mu_b(\dot{\gamma}^b)\,\dot{\gamma}_{xy}(\boldsymbol{U}_b)$, the general expressions (valid for any constitutive law of Reiner–Rivling type) of the $\boldsymbol{\tau}_k$ components are given as follows:

$$\tau_{1ij} = \left.\frac{\partial \tau_{ij}}{\partial \dot{\gamma}_{kl}}\right|_b \dot{\gamma}'_{kl} = (\mu_t - \mu_b)(\delta_{1i}\delta_{2j} + \delta_{2i}\delta_{1j})\dot{\gamma}'_{xy} + \mu_b \dot{\gamma}'_{ij}, \tag{3.16}$$

$$\begin{aligned}\tau_{2ij} = \frac{1}{2}\left[\frac{\partial^2 \tau_{ij}}{\partial \dot{\gamma}_{kl}\,\partial \dot{\gamma}_{mn}}\right]_b \dot{\gamma}'_{kl}\dot{\gamma}'_{mn} &= \frac{\mu_t - \mu_b}{4\dot{\gamma}^b}(\delta_{1i}\delta_{2j} + \delta_{2i}\delta_{1j})(\dot{\gamma}'_{mn})^2 + \frac{\mu_t - \mu_b}{\dot{\gamma}^b}\dot{\gamma}'_{ij}\dot{\gamma}'_{xy} \\ &\quad + \frac{1}{2}(\delta_{1i}\delta_{2j} + \delta_{2i}\delta_{1j})(\dot{\gamma}'_{xy})^2\left(\frac{\partial^2 \tau_b}{(\partial \dot{\gamma}^b)^2} - 3\,\frac{\mu_t - \mu_b}{\dot{\gamma}^b}\right),\end{aligned} \tag{3.17}$$

$$\begin{aligned}\tau_{3ij} = {} & \frac{\partial \mu_b}{\partial \dot{\gamma}^b}\frac{1}{2\,\dot{\gamma}^b}\left[(\delta_{1i}\delta_{2j} + \delta_{2i}\delta_{1j})\left((\dot{\gamma}'_{xy})^3 - \frac{1}{2}(\dot{\gamma}'_{kl})^2\dot{\gamma}'_{xy}\right) - (\dot{\gamma}'_{xy})^2\dot{\gamma}'_{ij} + \frac{1}{2}(\dot{\gamma}'_{pq})^2\dot{\gamma}'_{ij}\right] \\ & + \frac{1}{2}\frac{\partial^2 \mu_b}{(\partial \dot{\gamma}^b)^2}\left[(\delta_{1i}\delta_{2j} + \delta_{2i}\delta_{1j})\left(-(\dot{\gamma}'_{xy})^3 + \frac{1}{2}(\dot{\gamma}'_{kl})^2\dot{\gamma}'_{xy}\right) + (\dot{\gamma}'_{xy})^2\dot{\gamma}'_{ij}\right] \\ & + \frac{1}{6}\frac{\partial^3 \mu_b}{(\partial \dot{\gamma}^b)^3}\,\dot{\gamma}^b(\delta_{1i}\delta_{2j} + \delta_{2i}\delta_{1j})(\dot{\gamma}'_{xy})^3\end{aligned} \tag{3.18}$$

with δ_{ij} the Kronecker delta function and

$$\mu_t = \frac{\partial \tau_b}{\partial \dot{\gamma}^b}, \tag{3.19}$$

$$\frac{\partial \mu_b}{\partial \dot{\gamma}^b} = \frac{1}{\dot{\gamma}^b}\left(\frac{\partial \tau_b}{\partial \dot{\gamma}^b} - \frac{\tau_b}{\gamma^b}\right) = \frac{\mu_t - \mu_b}{\dot{\gamma}^b}, \tag{3.20}$$

$$\frac{\partial^2 \mu_b}{(\partial \dot{\gamma}^b)^2} = \frac{1}{\dot{\gamma}^b}\left[\frac{\partial^2 \tau_b}{(\partial \dot{\gamma}^b)^2} - \frac{2}{\dot{\gamma}^b}\left(\frac{\partial \tau_b}{\partial \dot{\gamma}^b} - \frac{\tau_b}{\dot{\gamma}^b}\right)\right], \tag{3.21}$$

$$\frac{\partial^3 \mu_b}{(\partial \dot{\gamma}^b)^3} = \frac{1}{\dot{\gamma}^b}\left[\frac{\partial^3 \tau_b}{(\partial \dot{\gamma}^b)^3} - 3\frac{1}{\dot{\gamma}^b}\frac{\partial^2 \tau_b}{(\partial \dot{\gamma}^b)^2} + \frac{6}{\dot{\gamma}^b}\left(\frac{\partial \tau_b}{\partial \dot{\gamma}^b} - \frac{\tau_b}{\dot{\gamma}^b}\right)\right]. \tag{3.22}$$

Here μ_t given by (3.19) corresponds to the tangent viscosity of the unidirectional base flow. For Bingham fluid, μ_t corresponds to the plastic viscosity and $\partial^2 \tau_b/(\partial \dot{\gamma}^b)^2 = \partial^3 \tau_b/(\partial \dot{\gamma}^b)^3 = 0$. The expressions of $\boldsymbol{\tau}_k$ $(k \leqslant 3)$, for the Bingham fluid case, are given in Appendix B.

Remarks. (i) The expressions (3.16)–(3.18) correspond to the shear stress perturbation, for which the development of the general Reiner–Rivling law has been carried out as a function of the $\dot{\gamma}$ invariants. One can notice that the terms factor of $(\delta_{1i}\delta_{2j}+\delta_{2i}\delta_{1j})$ correspond to anisotropic shear stress perturbation terms as they only appear in the xy components of $\boldsymbol{\tau}'$. A consequence of these anisotropic terms is that there is no equivalence to Squire's transformation for Bingham fluids (and for other nonlinear viscous fluids) unless unphysical restrictions are made (Georgievskii 1993). In other words, the three-dimensional case cannot be deduced from the bidimensional configuration as is done for Newtonian fluids. (ii) Here, the bilinear and trilinear forms of the shear stress tensor are only due to the viscosity perturbation.

The vorticity equation is obtained by calculating the curl of (2.1*b*). The knowledge of the linear, bilinear and trilinear forms of the stress tensor, permits determination of the different orders, in terms of the perturbation field, in the vorticity equation. Then, in the yielded regions, at first order, i.e. the linear operators of the perturbed vorticity equation are given by

$$\mathscr{D}_1 \equiv -\frac{1}{Pr}\Delta, \tag{3.23}$$

$$\mathscr{L}_{R1} \equiv -\Delta^2 + Re(U_b\partial_x\Delta - D^2U_b\,\partial_x) - 4B\,\partial_y\left(\frac{\partial_{xxy}}{\dot{\gamma}_b}\right), \tag{3.24}$$

where '∂_y' is replaced by 'D' for the functions depending only on y,

$$\mathscr{L}_{R2} \equiv Ra\,\partial_x. \tag{3.25}$$

One obtains the quadratic term as follows:

$$N_{21} = \frac{1}{Pr}[-\partial_y\psi\,\partial_x\nabla^2\psi + \partial_x\psi\,\partial_y\nabla^2\psi] + (\partial_{xx}-\partial_{yy})\tau_{2_{xy}}(\psi,\,\psi) + \partial_{xy}(\tau_{2_{yy}}(\psi,\,\psi) - \tau_{2_{xx}}(\psi,\,\psi)) \tag{3.26}$$

as well as the nonlinear cubic term given by

$$N_{31} = (\partial_{xx}-\partial_{yy})\tau_{3_{xy}}(\psi,\,\psi,\,\psi) + \partial_{xy}[\tau_{3_{yy}}(\psi,\,\psi,\,\psi) - \tau_{3_{xx}}(\psi,\,\psi,\,\psi)]. \tag{3.27}$$

The quadratic term (3.26) in the vorticity equation has an inertial contribution, such as the Newtonian case. For the non-Newtonian case, the quadratic and cubic terms have a viscosity-perturbation contribution, via the shear stress perturbation ($\boldsymbol{\tau}_2$ and $\boldsymbol{\tau}_3$ components). For readability reasons, the final expressions of N_{21} and N_{31} can be found in Appendix B. Since the nonlinear shear stress terms, or viscosity perturbation terms, are factor of B, for simplicity we would call these terms 'Bingham terms'.

3.3. *Energy equation*

Using the energy equation, written in terms of ψ and θ, the expressions of the linear operators, quadratic and cubic terms are easily identified:

$$\mathscr{D}_2 \equiv -1, \tag{3.28}$$

$$\mathscr{L}_{R3} \equiv -DT_b\partial_x, \tag{3.29}$$

$$\mathscr{L}_{R4} \equiv -\partial_{yy} - \partial_{xx} + PrReU_b\partial_x \tag{3.30}$$

and

$$N_{22} = -(\partial_y\theta)(\partial_x\psi) + (\partial_x\theta)(\partial_y\psi). \tag{3.31}$$

The energy equation does not contain any cubic terms, hence

$$N_{32} = 0. \tag{3.32}$$

3.4. *Perturbation modes*

3.4.1. *Assumptions*

Classically, the perturbation solution is sought as

$$\boldsymbol{V} = A(t)\,\mathrm{e}^{\mathrm{i}\alpha(x-ct)}\boldsymbol{V}_1(y) + \text{c.c.} + |A(t)|^2\,\boldsymbol{V}_0(y) + A(t)^2\,\mathrm{e}^{2\mathrm{i}\alpha(x-ct)}\boldsymbol{V}_2(y) + \text{c.c.}$$
$$+ |A(t)|^2\,A(t)\boldsymbol{V}_3(y)\,\mathrm{e}^{3\mathrm{i}\alpha(x-ct)} + \text{c.c.} + \cdots, \tag{3.33}$$

where $\boldsymbol{V}_n(y) = (f_n(y), \theta_n(y))^T$ and 'c.c.' means 'complex conjugate'. In the following, we use the notation $E^n = \mathrm{e}^{\mathrm{i}n\alpha(x-ct)}$. As the yield surfaces are determined via the stress field in the yielded zone, the perturbed yield surfaces have a similar form to $\boldsymbol{V}$:

$$Y^{\pm}(x,\,t) = AE^1Y_1^{\pm} + |A|^2\,Y_0^{\pm} + A^2E^2Y_2^{\pm} + |A(t)|^2A(t)\,Y_3^{\pm}\,E^3 + \text{c.c} + \cdots. \tag{3.34}$$

Developments (3.33)–(3.34) are assumed valid for Ra values close to the critical value Ra_c, i.e. $\epsilon = (Ra/Rac) - 1 \ll 1$. One can notice that in this study, the variations of the Rayleigh number, above criticality, are implicitly obtained by increasing $\delta\hat{T}$, the difference temperature between the two walls.

Moreover, it is assumed that the complex amplitude $A(t)$ evolves slowly with time and remains small. This last assumption is conditioned by the fact that the fundamental mode dominates the perturbation. Since no confusion is possible, we write A for $A(t)$, in the following.

The weakly nonlinear analysis consists in writing the system to the different amplitude orders identifying the terms in the modal basis E^n. In this paper, we consider the case $-3 \leqslant n \leqslant 3$.

3.4.2. *First order: fundamental*

The fundamental $\boldsymbol{V}_1 = (f_1, \theta_1)^T$ corresponds to the linear critical mode. The linear problem is defined by writing (3.1) to order $O(A)$:

$$c\,\mathscr{D}.(\boldsymbol{V}_1\,E^1) = \mathscr{L}_R.(\boldsymbol{V}_1\,E^1). \tag{3.35}$$

In the yielded region:

$$-\mathrm{i}\alpha\,c\begin{pmatrix}\mathscr{D}_1 & 0\\ 0 & -1\end{pmatrix}\begin{pmatrix}f_1\\ \theta_1\end{pmatrix} = \begin{pmatrix}\mathscr{L}_{R1} & \mathrm{i}\alpha Ra\\ \mathrm{i}\alpha & \mathscr{L}_{R4}\end{pmatrix}\begin{pmatrix}f_1\\ \theta_1\end{pmatrix}.$$

The operators $\mathscr{L}_{R1}$, $\mathscr{L}_{R3}$ and $\mathscr{D}_1$ read as follows:

$$\begin{cases}\mathscr{L}_{R1} \equiv +\mathrm{i}\alpha\,Re\,[U_b\,(D^2-\alpha^2) - D^2U_b] - (D^2-\alpha^2)^2 + 4\,\alpha^2\,BD\left(\dfrac{D}{|DU_b|}\right),\\ \mathscr{L}_{R4} \equiv \mathrm{i}\alpha\,Pr\,Re\,U_b - (D^2-\alpha^2),\\ \mathscr{D}_1 \equiv -\dfrac{1}{Pr}\,(D^2-\alpha^2).\end{cases}$$

In the unyielded region:

$$f_1 = 0, \tag{3.36}$$
$$\mathscr{L}_{R3}\,\theta_1 = c\,\theta_1. \tag{3.37}$$

The fundamental $\boldsymbol{V}_1$ satisfies the following boundary conditions. At the walls,

$$f_1(\pm 1/2) = Df_1(\pm 1/2) = 0 \tag{3.38}$$

and

$$\theta_1(\pm 1/2) = 0. \tag{3.39}$$

The linearized conditions (3.6) at the yield surfaces lead to

$$f_1(\pm y_b) = 0, \quad Df_1(\pm y_b) = 0, \tag{3.40}$$

$$D^2 f_1(\pm y_b) = \pm Y_1^{\pm} D^2 U_b(\pm y_b). \tag{3.41}$$

Remark. Equation (3.41) gives a condition for $Y_1^{\pm}$, not for f_1, considering the value of the derivative on the yielded side. If we consider the unyielded side, we obtain $D^2 f_1(\pm y_b) = 0$.

The solution of the system (3.35)–(3.41) is determined apart from an arbitrary multiplicative factor. In order to define a solution reference, we choose the following normalization:

$$\|\boldsymbol{V}_1\| = \frac{\mathrm{e}^{\mathrm{i}x_0}}{\|\boldsymbol{V}_1\|_\infty}\boldsymbol{V}_1, \tag{3.42}$$

with $\|\boldsymbol{V}_1\|_\infty = \max_y \sqrt{\mathrm{Re}(V_1)^2 + \mathrm{Im}(V_1)^2}$ the infinity norm, and the reference phase $x_0 = \arctan(-\mathrm{Im}(\|\boldsymbol{V}_1\|_\infty)/\mathrm{Re}(\|\boldsymbol{V}_1\|_\infty))$.

3.4.3. *Second order: quadratic modes*

The first harmonic is generated via the quadratic nonlinear terms. At $O(A^2)$, the interactions of the fundamental with itself or with its complex conjugate, respectively, lead to two different terms called modes 2 and 0. This section is devoted to the definition of these modes.

Mode 2, $\boldsymbol{V}_2 = (f_2, \theta_2)^T$, corresponds to the first harmonic of the perturbation and is produced by the interaction of the fundamental with itself in the quadratic nonlinear terms $\boldsymbol{N}_2(\boldsymbol{V}, \boldsymbol{V})$.

In the yielded region one can write

$$\mathscr{P}_{12} f_2 + 2\mathrm{i}\alpha\, Pr\, Re\, Ra\theta_2 = \mathscr{P}_{22}(f_1, f_1), \tag{3.43}$$

$$\mathscr{P}_{32}\theta_2 + 2\mathrm{i}\alpha f_2 = -\mathrm{i}\alpha(\theta_1\, Df_1 - D\theta_1\, f_1), \tag{3.44}$$

with

$$\begin{cases}
\mathscr{P}_{12} \equiv -2\mathrm{i}\alpha\, cRe\mathscr{P} + 2\mathrm{i}\alpha Pr Re^2[U_b\mathscr{P} - D^2U_b] - Pr Re\mathscr{P}^2 + 16\, B\, \alpha^2\, Pr Re\, D\left[\dfrac{D}{|DU_b|}\right], \\
\mathscr{P} \equiv D^2 - 4\alpha^2, \\
\mathscr{P}_{22}(f_1, f_1) = -Re\,\mathrm{i}\alpha(Df_1\, D^2 f_1 - f_1\, D^3 f_1) \\
\qquad\qquad + B\left(\dfrac{1}{\dot\gamma_b\, DU_b}\right)\left(10\,\alpha^4\,(Df_1)^2 + 8\,\alpha^4\, f_1\, D^2 f_1 + 9\,\alpha^2\,(D^2 f_1)^2\right. \\
\qquad\qquad \left. + 9\,\alpha^2\, Df_1\, D^3 f_1\right) + B\left(\dfrac{D^2U_b}{\dot\gamma_b\,(DU_b)^2}\right)(-16\,\alpha^4\, f_1\, Df_1 - 20\,\alpha^2\, Df_1\, D^2 f_1) \\
\qquad\qquad + B\left(\dfrac{(D^2U_b)^2}{\dot\gamma_b\,(DU_b)^3}\right)(3\,\alpha^2\,(Df_1)^2), \\
\mathscr{P}_{32} \equiv -2\mathrm{i}\alpha\, c + (Pr\, Re)2\mathrm{i}\alpha\, U_b - (D^2 - 4\alpha^2).
\end{cases}$$

In the plug region, the unyielded condition leads to

$$f_2 = 0. \tag{3.45}$$

At the walls, the no-slip condition and fixed temperature conditions are, respectively,

$$f_2(\pm 1/2) = 0, \tag{3.46}$$

$$\theta_2(\pm 1/2) = 0. \tag{3.47}$$

At the yield surfaces, $y = y_i^{\pm}$, the conditions can be written as follows:

$$2\,Df_2(\pm y_b) = (Y_1^{\pm})^2\,D^2U_b, \tag{3.48}$$

$$D^2f_2(\pm y_b) \pm Y_1^{\pm}\,D^3f_1(\pm y_b) \pm Y_2^{\pm}D^2U_b = 0, \tag{3.49}$$

$$f_2(\pm y_b) = 0. \tag{3.50}$$

Equations (3.48) and (3.50) allow the determination of f_2. Equation (3.49) is a condition for $Y_2^{\pm}$.

The interaction of the fundamental with its complex conjugate, in the nonlinear quadratic term $\boldsymbol{N}_2$, results in the first correction of the base flow to order $|A|^2$. It corresponds to the term $\boldsymbol{V}_0$ in (3.33). By definition, it does not depend on the x coordinate.

In order to satisfy the mass conservation, the velocity of mode 0 takes the form $\boldsymbol{u}_0 = (u_0(y),\ 0)^T$. In this respect, it seems more natural to consider the velocity rather than the streamfunction for this mode.

In the yielded region, one considers fixed pressure gradient conditions, i.e. $\langle \partial_x p_0 \rangle_x = 0$, where $\langle \bullet \rangle_x \equiv 1/2X \int_{-X}^{X} \bullet \,\mathrm{d}x$, and a quasi-stationary assumption. Then, the averaged momentum conservation, with respect to x, identified in terms of 'E^0' to order $|A|^2$, is given by

$$(Pr\,Re)\,D^2u_0 = \mathrm{i}\alpha Re(f_{-1}\,D^2f_1 - f_1\,D^2f_{-1}) + B\alpha^2 D\left(\frac{Df_1\,Df_{-1}}{DU_b\,\dot{\gamma}_b}\right). \tag{3.51}$$

In (3.51), one notices that u_0 comes from an inertial term f_{In} such as in the Newtonian case and from an additional Bingham term f_B:

$$f_{In} = \mathrm{i}\alpha(f_{-1}\,D^2f_1 - f_1\,D^2f_{-1}) \tag{3.52}$$

and

$$f_B = \alpha^2 D\left(\frac{Df_1\,Df_{-1}}{DU_b\,\dot{\gamma}_b}\right). \tag{3.53}$$

In the plug region, the condition $\dot{\gamma}_{ij} = 0$ leads to

$$\partial_x u_0 = \partial_y u_0 = 0, \tag{3.54}$$

then

$$u_0 = \text{const.} \tag{3.55}$$

The heat equation, to order $|A|^2$, reads

$$D^2\theta_0 = \mathrm{i}\alpha(\theta_1\,Df_{-1} - \theta_{-1}\,Df_1 + f_{-1}\,D\theta_1 - f_1\,D\theta_{-1}). \tag{3.56}$$

The boundary conditions at the walls are given by

$$u_0(\pm 1/2) = 0 \quad \text{and} \quad \theta_0(\pm 1/2) = 0. \tag{3.57}$$

At the yield surfaces, the conditions are given by

$$Du_0|_{\pm y_b} \pm Y_0^{\pm}D^2U_b \pm Y_1^{\pm}\,D^3f_{-1}(\pm y_b) \pm Y_{-1}^{\pm}\,D^3f_1(\pm y_b) = 0. \tag{3.58}$$

The additional needed conditions come from momentum-conservation equilibrium on a plug-zone element $\Omega_s = [d - X; d + X] \times [y_i^-; y_i^+]$, with d being a constant:

$$\frac{\mathrm{d}}{\mathrm{d}t}\int\int\int_{\Omega_s}(\boldsymbol{u})_i\,\mathrm{d}\mathscr{V} = \oint_{\delta\Omega_s}\sigma_{ij}(\boldsymbol{U_b}+\boldsymbol{u})\boldsymbol{e_j}\,\mathrm{d}S + \int\int\int_{\Omega_s} Ra\,(T_b+\theta)\boldsymbol{e_y}\,\mathrm{d}\mathscr{V}. \quad (3.59)$$

Manipulation of this vector equation leads to

$$[Du_0]_{-y_b}^{y_b} = -\alpha^2 B(|Y_1^+|^2 + |Y_1^-|^2) - 2(Y_1^+ D^3 f_{-1}(y_b) + Y_{-1}^+ D^3 f_1(y_b)), \quad (3.60)$$

$$Ra\, y_b(Y_0^+ - Y_0^-) = Ra[Y_1^+\theta_{-1}(y_b) + Y_{-1}^+\theta_1(y_b) + Y_1^-\theta_{-1}(-y_b) + Y_{-1}^-\theta_1(-y_b)] + Ra\frac{y_b^2}{2}\alpha_c^2(|Y_1^+|^2 - |Y_1^-|^2). \quad (3.61)$$

Calculations are detailed in Appendix C. Combining (3.58), (3.60) and (3.61), one obtains $Y_0^+ + Y_0^-$ and $Y_0^+ - Y_0^-$:

$$Y_0^+ + Y_0^- = \frac{1}{D^2 U_b}[Y_1^+ D^3 f_{-1}(y_b) - Y_1^- D^3 f_{-1}(-y_b) + Y_{-1}^+ D^3 f_1(y_b) - Y_{-1}^- D^3 f_1(-y_b)] - \frac{1}{D^2 U_b}[\alpha^2 B(|Y_1^+|^2 + |Y_1^-|^2)] \quad (3.62)$$

and

$$(Y_0^+ - Y_0^-) = \frac{1}{y_b}(Y_1^+\theta_{-1}(y_b) + Y_{-1}^+\theta_1(y_b) + Y_1^-\theta_{-1}(-y_b) + Y_{-1}^-\theta_1(-y_b)) + \frac{y_b\alpha^2}{2}(|Y_1^+|^2 - |Y_1^-|^2). \quad (3.63)$$

3.5. *Third-order solution and the amplitude equation*

The third-order solution, in particular the cubic mode $\boldsymbol{V}_3 = (f_3, \theta_3)^T$, permits determination of the amplitude equation. Substituting (3.33) in (3.1) and identifying the terms factor of E^1, one obtains

$$|A|^2 A(\mathscr{L}_R + \mathrm{i}\alpha\, c\,\mathscr{D})\boldsymbol{V}_3 = \partial_t A\,\mathscr{D}\boldsymbol{V}_1 - A\,(\mathscr{L}_R + \mathrm{i}\alpha\, c\,\mathscr{D})\,\boldsymbol{V}_1 - \mathscr{M}_1(N_2(\boldsymbol{V},\boldsymbol{V}) + N_3(\boldsymbol{V},\boldsymbol{V},\boldsymbol{V})), \quad (3.64)$$

where the notation $\mathscr{M}_i(\bullet)$, for $i = 0, 1, 2, 3$ corresponds to the identification of $\bullet$ in terms of mode i, i.e. E^i and

$$\mathscr{M}_1(N_2(\boldsymbol{V},\boldsymbol{V}) + N_3(\boldsymbol{V},\boldsymbol{V},\boldsymbol{V})) = E^{-1}|A|^2 A\,([N_2(\boldsymbol{V}_{-1}E^{-1}, \boldsymbol{V}_2E^2)] + [N_2(\boldsymbol{V}_1E^1, \boldsymbol{V}_0)]) + E^{-1}(|A|^2 A\,[N_3(\boldsymbol{V}_1E^1, \boldsymbol{V}_1E^1, \boldsymbol{V}_{-1}E^{-1})]), \quad (3.65)$$

$$(\mathscr{L}_R + \mathrm{i}\alpha\, c\,\mathscr{D})\,\boldsymbol{V}_1 = \frac{1+\mathrm{i}S}{t_c}\epsilon\,\mathscr{D}\boldsymbol{V}_1. \quad (3.66)$$

Remark. The term $((1+\mathrm{i}S)/t_c)$ comes from the growing rate $\sigma = -\mathrm{i}\alpha\, c$ for which a Taylor expansion about criticality is written. To first order, it reads

$$\sigma = -\mathrm{i}\omega_c + \frac{1+\mathrm{i}S}{t_c}\epsilon + O(\epsilon^2), \quad (3.67)$$

with the critical pulsation $\omega_c = \alpha_c\, c$ and the characteristic time $t_c = 1/\mathrm{Re}(\sigma) > 0$.

The boundary conditions for $\boldsymbol{V}_3$ are obtained as for the previous modes and are given by

$$f_3(\pm 1/2) = Df_3(\pm 1/2) = 0, \tag{3.68}$$

$$f_3(\pm y_b) = 0, \tag{3.69}$$

$$Df_3(\pm y_b) = \mp Y_0^{\pm} D^2 f_1(\pm y_b) + \frac{(Y_1^{\pm})^2}{2} D^3 f_{-1}(\pm y_b) - Y_1^{\pm} Y_{-1}^{\pm} D^3 f_1(\pm y_b). \tag{3.70}$$

One notices that the boundary conditions at the yield surfaces (defined in (3.70)) are inhomogeneous. In order to derive the Fredholm solvability conditions we first introduce, as in Gross (2002), a new variable $\boldsymbol{V}_{3H}$ to produce homogeneous boundary conditions:

$$\boldsymbol{V}_{3H} = \boldsymbol{V}_3 - \boldsymbol{V}_{3NH}, \tag{3.71}$$

with $\boldsymbol{V}_{3NH}$ and $\boldsymbol{V}_{3H} \in [\mathscr{C}^2(\Omega)]$ and $\Omega = [-X; X] \times [-1/2; 1/2]$. Furthermore, $\boldsymbol{V}_{3NH}$ is a function characterized by same boundary conditions as the $\boldsymbol{V}_3$ ones. Substituting $\boldsymbol{V}_3 = \boldsymbol{V}_{3H} + \boldsymbol{V}_{3NH}$ in (3.64), we obtain

$$|A|^2 A(\mathscr{L}_R + \mathrm{i}\alpha\, c\, \mathscr{D})\boldsymbol{V}_{3H} = \partial_t A\, \mathscr{D}\boldsymbol{V}_1 - A(\mathscr{L}_R + \mathrm{i}\alpha\, c\, \mathscr{D})\boldsymbol{V}_1 - \mathscr{M}_1(N_2(\boldsymbol{V}, \boldsymbol{V}) + N_3(\boldsymbol{V}, \boldsymbol{V}, \boldsymbol{V})) - |A|^2 A(\mathscr{L}_R + \mathrm{i}\alpha\, c\, \mathscr{D})\boldsymbol{V}_{3NH}. \tag{3.72}$$

The Fredholm alternative theorem states that (3.72), with the homogeneous boundary conditions, has a solution if the inhomogeneity (right-hand side of (3.72)) is orthogonal to the null space of the adjoint operator (the adjoint operator is defined as in Schmid & Heningson 2001, and is detailed in Appendix D). Therefore, the Hermitian scalar product of (3.72) with the adjoint mode leads to the amplitude equation, i.e. the complex Landau equation,

$$\partial_t A = \epsilon \frac{1 + \mathrm{i}S}{t_c} A + \lambda_1 |A|^2 A, \tag{3.73}$$

with λ_1 the Landau coefficient,

$$\lambda_1 = \frac{1}{\langle \mathscr{D}.\boldsymbol{V}_1 E^1, \boldsymbol{V}_{adj} \rangle} \langle [N_2(\boldsymbol{V}_{-1} E^{-1}, \boldsymbol{V}_2 E^2)] + [N_2(\boldsymbol{V}_1 E^1, \boldsymbol{V}_0)], \boldsymbol{V}_{adj} \rangle + \frac{1}{\langle \mathscr{D}.\boldsymbol{V}_1 E^1, \boldsymbol{V}_{adj} \rangle} \langle [N_3(\boldsymbol{V}_1 E^1,\ \boldsymbol{V}_1 E^1,\ \boldsymbol{V}_{-1} E^{-1})], \boldsymbol{V}_{adj} \rangle + \lambda_{NH} \tag{3.74}$$

and

$$\lambda_{NH} = -\frac{|A|^2 A}{\langle \mathscr{D}.\boldsymbol{V}_1 E^1, \boldsymbol{V}_{adj} \rangle} \langle (\mathscr{L}_R + \mathrm{i}\alpha\, c\, \mathscr{D})\boldsymbol{V}_{3NH}, \boldsymbol{V}_{adj} \rangle \tag{3.75}$$

$$= -\frac{1}{\langle \mathscr{D}.\boldsymbol{V}_1 E^1, \boldsymbol{V}_{adj} \rangle} [Df_3\, D^2 f_{adj}]_{-y_b}^{y_b}. \tag{3.76}$$

In these equations, the Hermitian scalar product is defined by

$$\langle \boldsymbol{V}, \boldsymbol{W} \rangle = \int \frac{1}{\mathscr{V}} \boldsymbol{V} \cdot \boldsymbol{W}^* \, \mathrm{d}\Omega, \tag{3.77}$$

with $\mathscr{V}$ the volume of the domain Ω and W^* the complex conjugate of W.

One notices that λ_{NH} comes from the $\boldsymbol{V}_{3NH}$ inhomogeneous conditions at $y = \pm y_b$ like those given by (3.70). In the following, we also adopt the notation

$$\lambda_1 = -g_1(1 + \mathrm{i}C), \tag{3.78}$$

where g_1 and C are real.

4. Results and discussion

4.1. *Numerical method*

In order to attain the convergence of the whole extensive results leading to the Landau coefficient λ_1 (3.74), an accurate numerical method is used. In particular, the boundary conditions involve some third-order derivatives which require high accuracy in calculations. In this respect, the discretization of the system (3.1) subject to its boundary conditions is done by means of a fourth-order-centred finite scheme.

The discretized linear problem leads to an eigenvalue problem, with c the eigenvalue, which is solved by using the QZ algorithm implemented in the Matlab 7.1 software package. The Hermitian scalar products involved in the determination of the Landau coefficient (3.74) are evaluated by means of the Simpson method.

The numerical code has been tested for the Newtonian case. The critical conditions obtained via the Newtonian linear problem are compared with the ones computed by Nicolas (2002). The discrepancy is less than 1 %. Concerning the weakly nonlinear analysis, our results are compared with those obtained by Müller *et al.* (1989). For the case $Pr = 1$, we recover a supercritical bifurcation ($g_1 > 0$) and that the coefficient C – given in (3.78) – varies linearly with the Reynolds number. Moreover, for $N = 201$, we found $C = 0.0108\, Re_m$, with Re_m the Reynolds number scaled with the mean velocity. This coefficient is comparable to the one obtained by Müller: $C = 0.0113\, Re_m$.

The convergence of our numerical scheme has been tested in the computation of the perturbation modes (linear and quadratic) and the Landau coefficient. Converging results are obtained for $N = 801$ grid points.

4.2. *Linear modes*

The linear stability analysis of this flow leads to propagating convective patterns, on both sides of the plug zone, in the form of travelling waves. Marginal stability curves are displayed in figure 3 for different values of B. The stabilizing effect of the yield stress is clearly highlighted. It was shown by Métivier & Nouar (2008) that the increase in the critical Rayleigh number Ra_c with increasing B is mainly dominated by the reduction of the yielded zone width if $y_b < 0.25$ and by the increase in the effective viscosity if $y_b > 0.25$. In both cases, the viscosity stratification has a weak influence on the critical conditions.

The structure of the perturbation is represented via the eigenmodes in terms of temperature and streamfunction (figure 4). The isovalues of temperature and streamfunction perturbation on a period along x permit characterization of the contra-rotative rolls on both sides of the plug zone (figure 5).

Moreover, figure 6 represents the yield surface perturbation of the linear mode for different values of y_b. One notices that the maximal value of the perturbation, in terms of the yield surface position, decreases with increasing y_b, meaning that the perturbation of the plug region is smaller for increasing Bingham numbers. Furthermore, the perturbed positions of the upper and lower yield surfaces have the same sign and value at fixed x position. It means that the perturbation of the plug region corresponds to sinuous modes.

4.3. *Quadratic modes*

4.3.1. *Mode 2*

The first harmonic of the perturbation, i.e. the quadratic mode 2, is calculated from the system (3.43)–(3.50). Results concerning mode 2 are displayed in figure 7, in which the streamfunction $f_2(y)$ and temperature $\theta_2(y)$ profiles are plotted.

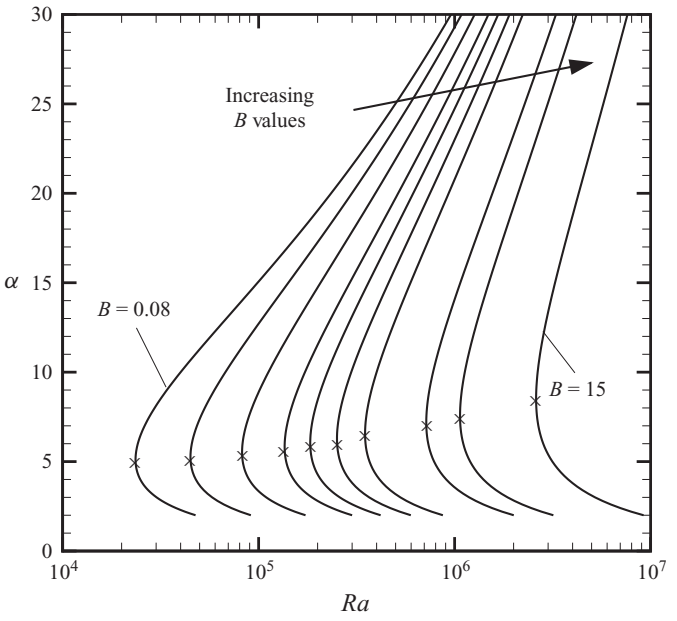

FIGURE 3. Marginal curves: numerical results for the case $Re = 0.01$, $Pr = 50$ and different values of B (or y_b) varying from 0.08 to 15 (or 0.01–0.3 for y_b); $\times$ corresponds to the critical conditions $(\alpha_c,\ Ra_c)$.

Figure 8 shows the structure of the perturbations via the isovalues of the streamfunction $\psi_2(x,\ y)\,E^2$ and the temperature $\theta_2(x,\ y)\,E^2$ in the $(x,\ y)$ plane, for one x-period $2\pi/\alpha$. One recovers for the harmonic the same structure as the fundamental mode, i.e. the convective patterns on both sides of the plug region. Obviously, one notices the increasing rolls number since by definition the mode 2 wavelength is half the fundamental one.

Finally, the yield surface perturbation is displayed in figure 9. One observes that mode 2 is not negligible. Indeed, for the range of tested values, this quadratic mode can be 100 times larger than the fundamental one, in terms of streamfunction temperature and yield surface position. This observation reveals the great importance of nonlinearities above criticality. This point is discussed in the following sections for the whole quadratic mode (modes 2 and 0).

4.3.2. *Mode 0*

Mode 0 is obtained by solving the system of equations (3.51)–(3.56) with the appropriate boundary conditions (3.58)–(3.63). This harmonic corresponds to the first perturbation correction of the base flow.

Velocity and temperature profiles of this mode are presented in figure 10. One notices that the velocity u_0 takes negative values, which means that the primary flow tends to be slowed down. This effect is stronger for increasing B values. In addition, the width of the unyielded region increases with the perturbation as shown in figure 11. The u_0 negative values and Y_0^+ positive ones have opposite contributions to the instabilities evolution. Indeed, the first one destabilizes the flow and the second one corresponds to a stabilizing effect.

At the onset of the Rayleigh–Bénard rolls, the convective heat transfer is enhanced, leading to the reduction of the temperature difference between the wall and the yield

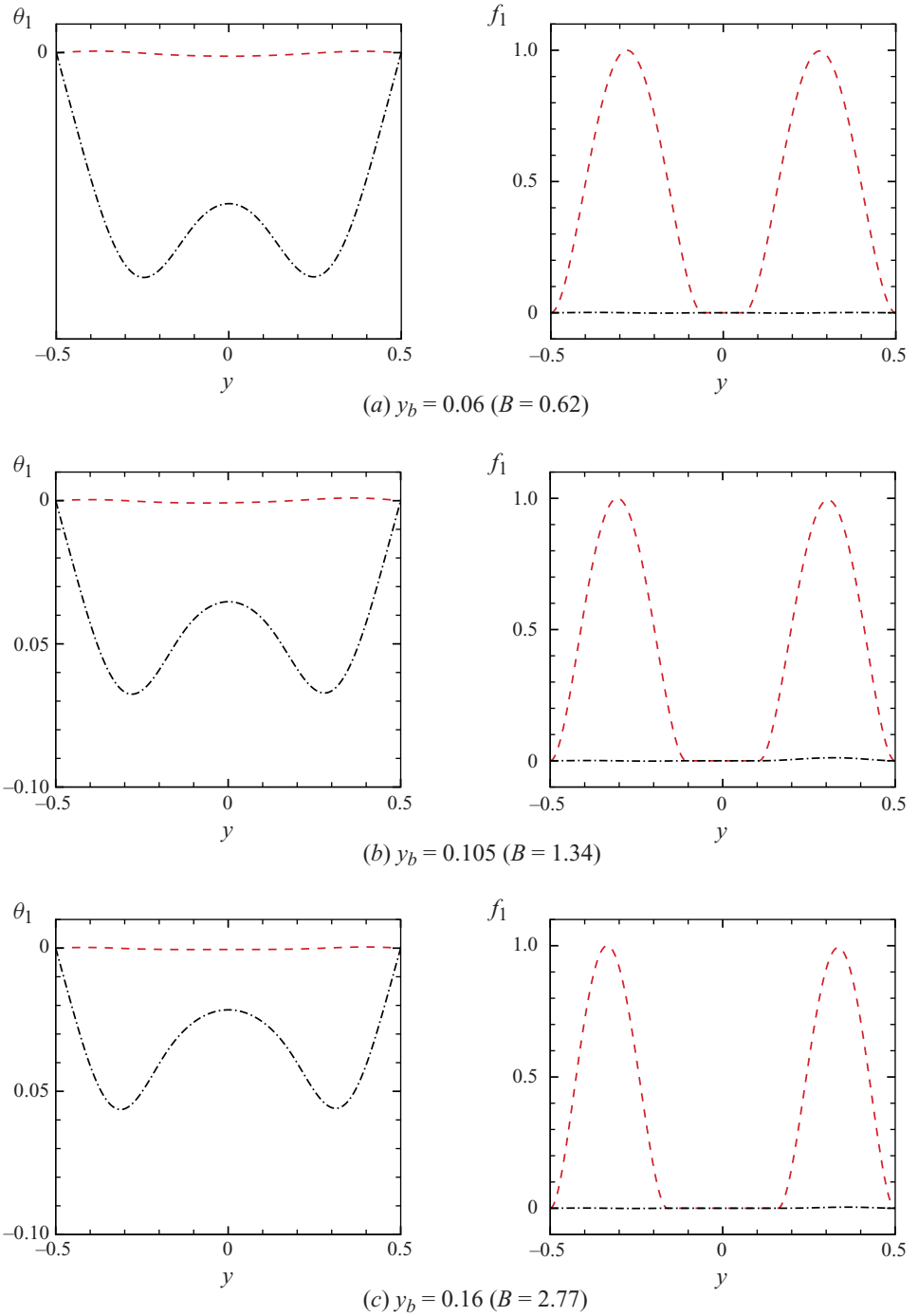

FIGURE 4. (Colour online) Fundamental mode at criticality: temperature (left) and streamfunction (right); - - -, real parts; —·—·—, imaginary parts. Numerical results for $Re = 0.02$ and $Pr = 50$.

surface as is shown by the temperature profiles θ_0 in figure 10(b). In other words, θ_0, the modification to order $|A|^2$ of the conductive temperature profile T_b improves the heat transfer in the yielded regions.

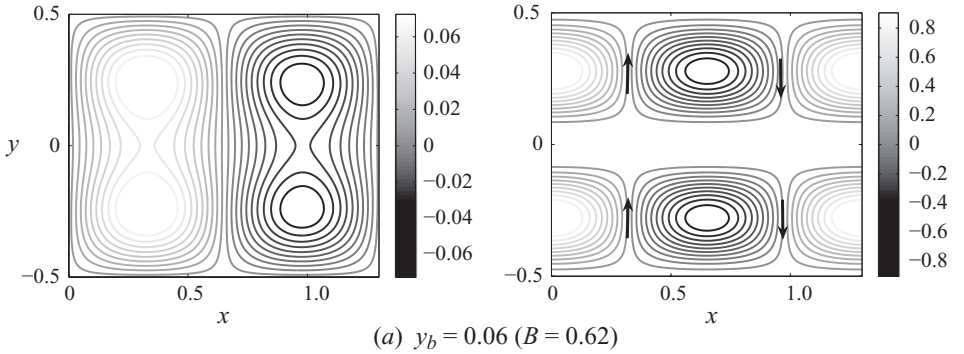

(*a*) $y_b = 0.06$ ($B = 0.62$)

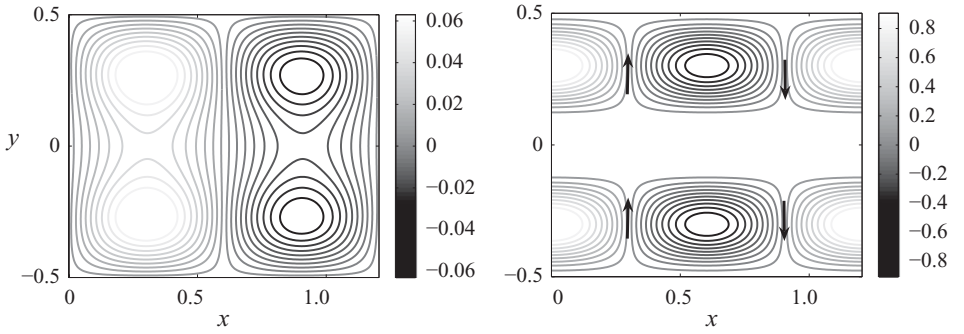

(*b*) $y_b = 0.105$ ($B = 1.34$)

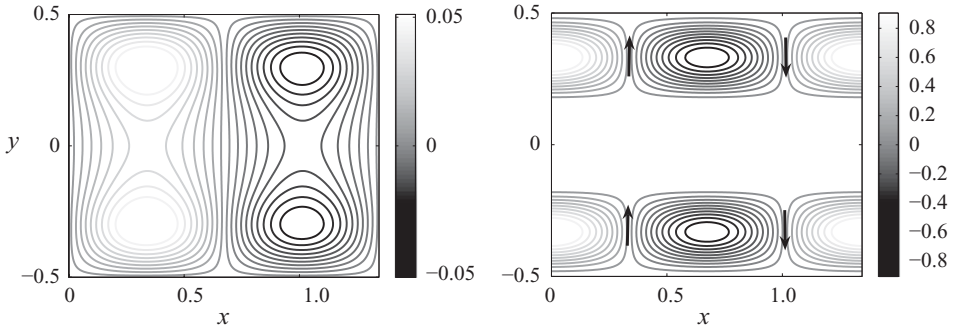

(*c*) $y_b = 0.16$ ($B = 2.77$)

FIGURE 5. Isovalues of temperature (left) and streamfunction (right) represented on one period along x for different values of y_b. The arrows indicate the rotation direction of the rolls.

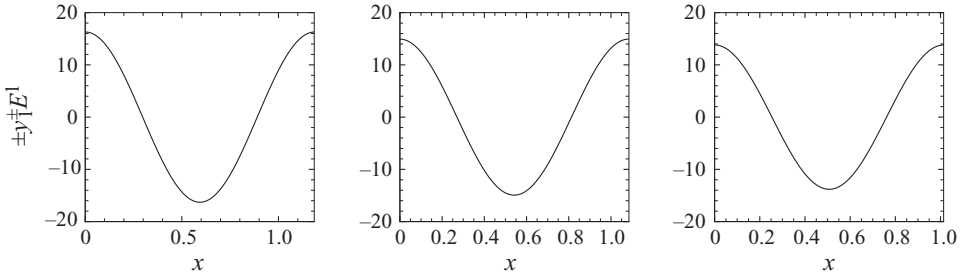

(*a*) $y_b = 0.06$ ($B = 0.62$) (*b*) $y_b = 0.105$ ($B = 1.34$) (*c*) $y_b = 0.16$ ($B = 2.77$)

FIGURE 6. Mode 1 yield surface perturbations for the case $Re = 0.02$ and $Pr = 50$.

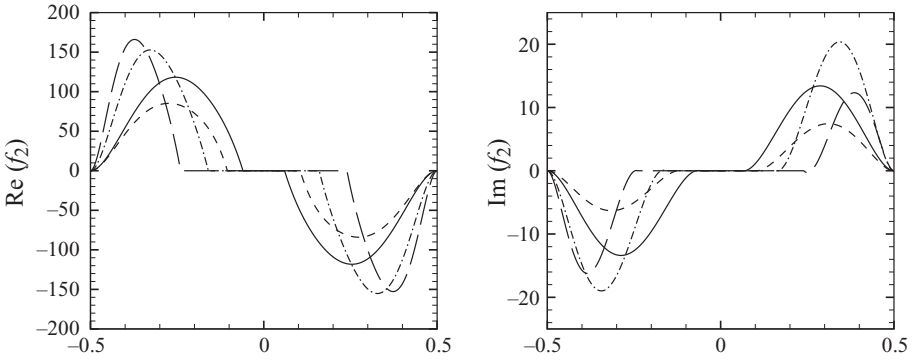

(a) Mode 2: real and imaginary parts of the streamfunction

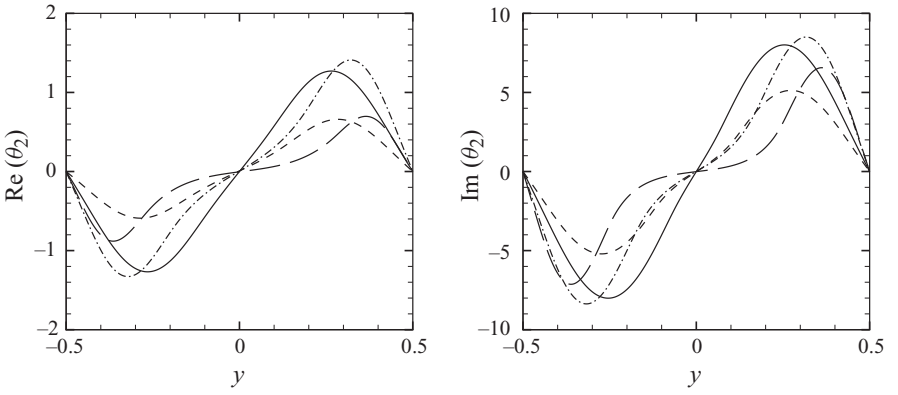

(b) Mode 2: real and imaginary parts of the temperature

FIGURE 7. Mode 2 perturbations in terms of streamfunction (a) and temperature (b): numerical results for the case $Re = 0.02$ and $Pr = 50$. Solid lines, $y_b = 0.06\,(B = 0.62)$; dashed lines, $y_b = 0.105\,(B = 1.34)$; dot-dashed lines, $y_b = 0.16\,(B = 2.77)$, long-dashed lines, $y_b = 0.24\,(B = 7.1)$.

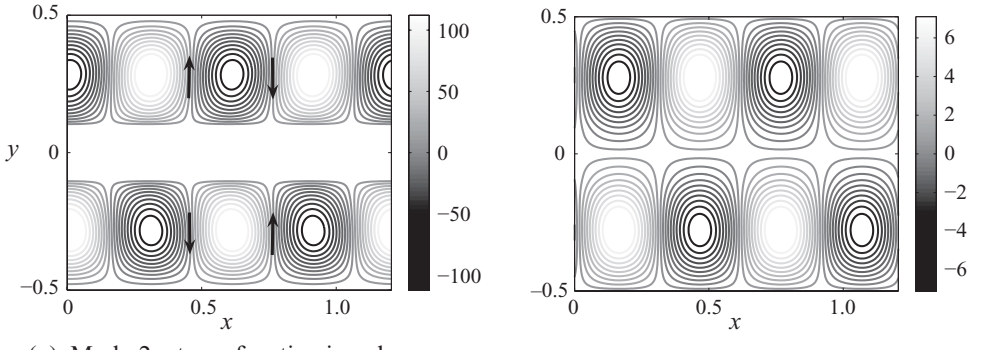

(a) Mode 2: streamfunction isovalues

(b) Mode 2: temperature isovalues

FIGURE 8. Mode 2 perturbation: isovalues of the streamfunction (a) and temperature (b) in the (x, y) plane for one period. The arrows indicate the rotation direction of the rolls. Numerical results for the case $y_b = 0.105\,(B = 1.34)$, $Re = 0.02$ and $Pr = 50$.

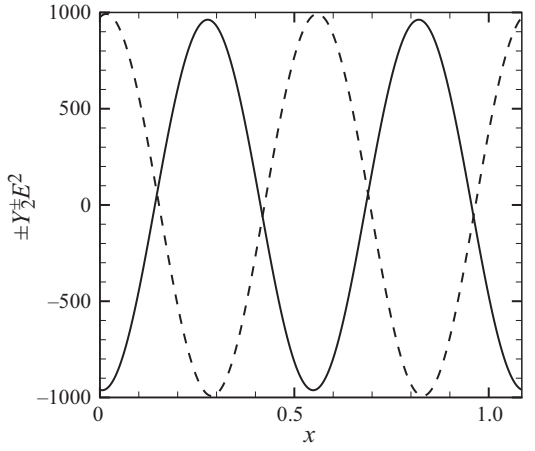

FIGURE 9. Yield surface perturbation of mode 2. Solid lines, upper interface $Y_2^+ E^2$; dashed lines, lower interface $-Y_2^- E^2$; for $Re = 0.02$, $Pr = 50$, $y_b = 0.105$ ($B = 1.34$).

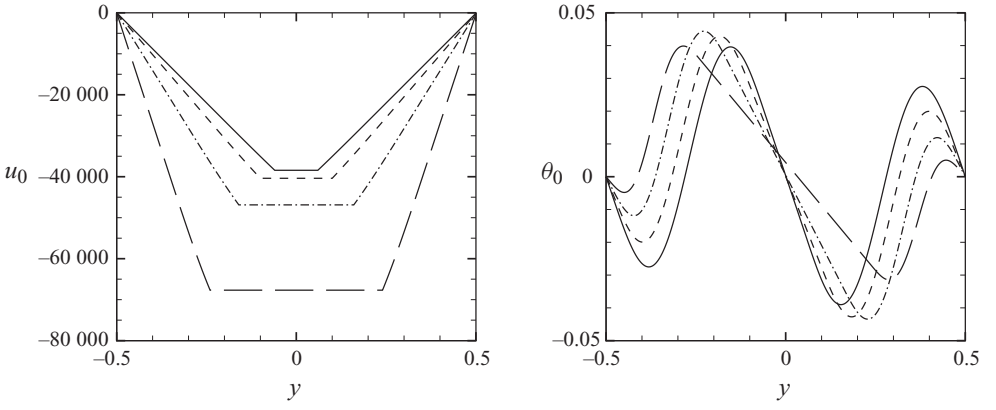

(*a*) Mode 0: velocity (*b*) Mode 0: temperature

FIGURE 10. Mode 0 perturbation: velocity (*a*) and temperature (*b*) profiles. Numerical results for the case $Re = 0.02$ and $Pr = 50$. Solid lines, $y_b = 0.06$ ($B = 0.62$); dashed lines, $y_b = 0.105$ ($B = 1.34$); dot-dashed lines, $y_b = 0.16$ ($B = 2.77$); long-dashed lines, $y_b = 0.24$ ($B = 7.1$).

As in mode 2, one can highlight the high values taken by mode 0 compared with the fundamental one. Indeed, in the case presented in figure 10(*a*), u_0 reaches values of the order $O(10^4)$. The velocity u_0 has an inertial and a viscous origin via f_{In} and f_B, respectively, as previously defined by (3.51)–(3.53). In figure 12, the nonlinear quadratic effects f_{In} and f_B are represented in the lower yielded region as a function of a rescaled y-coordinate. Results are displayed for fixed Reynolds and Prandtl numbers $Re = 0.02$, $Pr = 50$ and different y_b values. In the light of figure 12, one can clearly infer the dominant effect of the nonlinear viscous terms compared with the nonlinear inertia terms. Moreover, one can notice that, for $|y^*| < 0.26$, the function f_B increases strongly and reaches a maximum at the lower yield surface ($y^* = 0$). The maximal value attained by f_B increases with the yield stress value. The strong variation of f_B characterizes the importance of the nonlinear variation of the effective viscosity with the shear rate, particularly near the yield surface. In other words, the

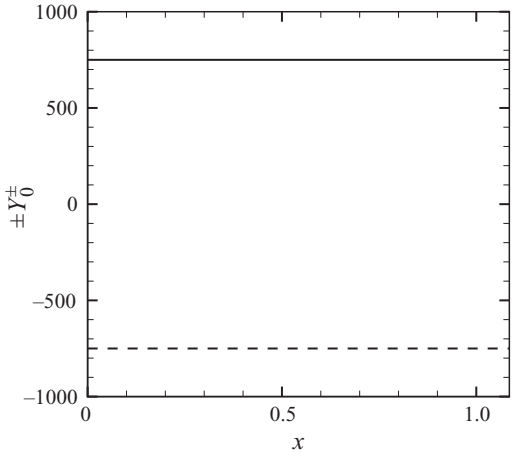

FIGURE 11. Mode 0 yield surface perturbation: Y_0^+ (upper solid interface) and $-Y_0^-$ (lower dashed interface). Case $Re = 0.02$, $Pr = 50$, $y_b = 0.105\,(B = 1.34)$.

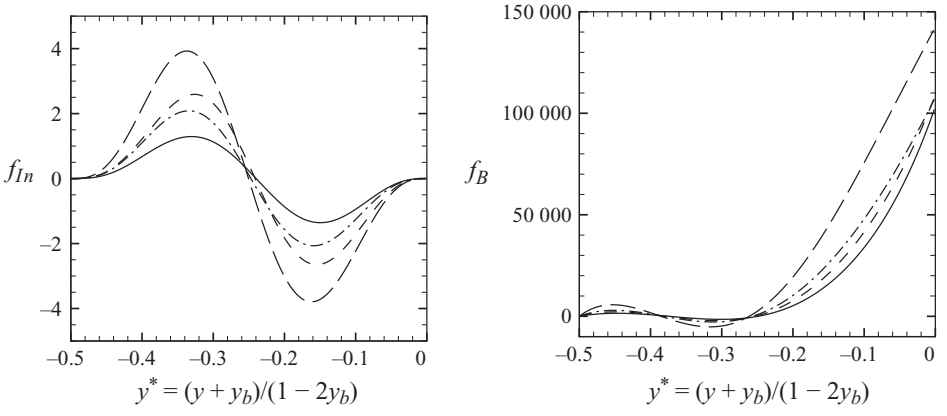

FIGURE 12. Effect of the inertia and viscosity on u_0 through the representation of f_{In} (left) and f_B (right) in the lower yielded region. Solid lines, $y_b = 0.06\,(B = 0.62)$; dashed lines, $y_b = 0.105\,(B = 1.34)$; dot-dashed lines, $y_b = 0.16\,(B = 2.77)$; long-dashed lines, $y_b = 0.24$ $(B = 7.1)$). Numerical results for $Pr = 50$ and $Re = 0.02$.

nonlinear variation of the fluid viscosity generates large nonlinear perturbations via the quadratic modes.

Remark. Quadratic modes have only been displayed for the case $Re = 0.02$, $Pr = 50$ since numerical results indicate that the quadratic modes are not really sensitive to weak variations of the Re and Pr values, i.e. $\Delta Re \sim O(10^{-2})$ and $\Delta Pr \sim O(1)$. Tendencies similar to those presented in figures 8 and 10 are observed by varying the Reynolds and Prandtl values.

4.4. *Range of validity of the weakly nonlinear analysis*

Considering large quadratic modes, the validity of the analysis has to be discussed. Indeed, the validity of the limited solution, terminated after the quadratic order, is

y_b	g_1	C	t_c	$\frac{\omega_m}{\epsilon} = \frac{C-S}{t_c}$	ω_c
0.04	11 541 379.7	−13.08	0.0092	−1421.08	4.38
0.06	28 694 943.4	−12.77	0.0213	−978.78	3.95
0.1	377 332 679	−4.80	0.015	−312.44	4.92
0.14	609 062 444.5	−4.14	0.0146	−282.68	4.74
0.16	928 126 236.8	−3.38	0.0138	−245.21	5.01
0.2	1 961 341 646	−2.39	0.0090	−264.97	5.51
0.24	3 823 418 847	−2.25	0.0092	−255.86	5.61

TABLE 1. Numerical values of the different coefficients involved in the determination of the amplitude evolution, $Pr = 50$, $Re = 0.02$.

conditioned by a dominant fundamental mode with respect to the harmonics, i.e. $|A\,\boldsymbol{V}_1| \gg |A_k\,\boldsymbol{V}_k|$, for $k \neq \pm 1$. In order to satisfy this assumption, a condition on the amplitude modulus is imposed as follows:

$$|A| \ll \frac{\max(|\boldsymbol{V}_1)|}{\max(|\boldsymbol{V}_0|, |\boldsymbol{V}_2|)}. \tag{4.1}$$

Following Malkus *et al.* (1958), one can limit the ratio given by (4.1) to a maximal value of 0.1. On the other hand, numerical results indicate that the maximal value of the quadratic modes is reached by mode 0. Therefore, for the range of results obtained, condition (4.1) implies $|A| \ll O(10^{-4})$. This weak value indicates that the weakly nonlinear stability of the Bingham RBP flow has an extremely narrow range of validity. This result is comparable to the one obtained for the Newtonian case. Actually, Kuo (1961) and more recently, Generalis & Fujimura (2009) have compared results obtained via a weakly nonlinear analysis and via a nonlinear analysis in the Newtonian Rayleigh–Bénard configuration for finite Prandtl values and low Prandtl values respectively. The authors show that the weakly nonlinear analysis has a limited range of validity: as a consequence, the number of perturbation modes has to be increased rapidly in order to describe correctly the amplitude evolution. Concerning the Newtonian-plane-Poiseuille stability flow, Herbert (1980) has numerically shown that the range of validity is very narrow. Indeed, the convergence of the Stuart–Landau equation requires considerably small $|A|$ which does not violate the assumption of the weak nonlinearity. In this case, the narrow range of validity is certainly due to the subcritical nature of the bifurcation in the plane-Poiseuille-flow case.

In this paper, the really narrow range of validity is a consequence of the large variations of viscosity in the yielded regions. In addition, these weak amplitude values permit one to confirm that the plug region does not break up, which is an implicit assumption.

4.5. *Amplitude evolution*

The amplitude perturbation evolution $A(t)$ depends on the sign of g_1 defined by (3.73) and (3.78). Numerical results obtained for $Pr = 50$, $Re = 0.02$ and different y_b values are given in table 1. For this range of values, one finds that g_1 takes positive values meaning a supercritical bifurcation. One can observe that g_1 increases with the increase in B, i.e. the increase in the degree of the nonlinearity of rheological behaviour of the fluid. Physically, large values of g_1 are linked to the sensitivity of the

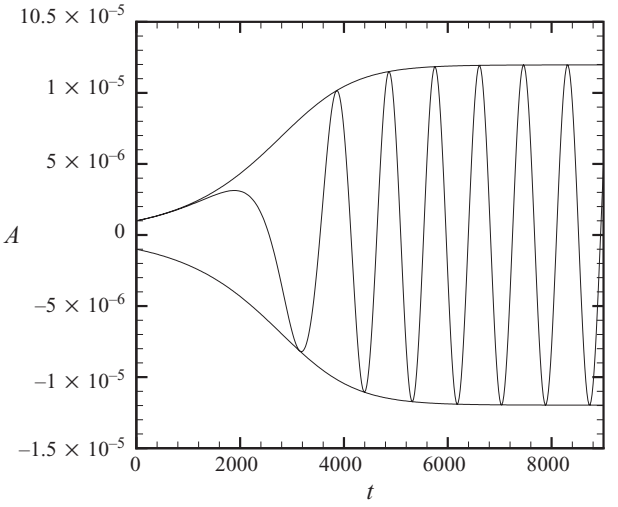

FIGURE 13. Amplitude evolution as a function of time above criticality for a supercritical bifurcation case.

system with respect to strong variations of the viscosity with the shear rate. Indeed, in the range of low shear rate, a small perturbation may induce a large viscosity perturbation.

In the supercritical bifurcation case, above criticality, the perturbation amplitude increases with time and reaches a saturated value A_c.

Using a polar representation of the amplitude,

$$A = \rho\, \mathrm{e}^{\mathrm{i}\phi}, \tag{4.2}$$

one obtains the saturated amplitude,

$$\rho = |A_c| = \sqrt{\frac{\epsilon}{t_c\, g_1}}, \tag{4.3}$$

and the phase,

$$\phi = \phi_0 - \omega_m\, t, \tag{4.4}$$

with ϕ_0 an initial value and

$$\omega_m = \frac{C - S}{t_c}\,\epsilon = g_1(C - S)|A_c|^2, \tag{4.5}$$

where ω_m corresponds to a correction of the fundamental pulsation $\omega_c = \alpha_c\, c$.

Equation (4.4) highlights the amplitude oscillations with time, as displayed in figure 13. Numerical results indicate that for fixed values of $\epsilon = (Ra - Ra_c)/Ra$, the saturated amplitude A_c decreases for increasing Bingham numbers. In other words, for fixed ϵ values, the increase in B limits the saturated amplitude which corresponds to a stable bifurcation branch. This is a direct consequence of the increase in g_1 with the increase in the degree of the nonlinearity in the Bingham model. This is in agreement with the results obtained by Cheng & Lai (2008).

The critical pulsation ω_c is given in table 1 as well as the values of ω_m/ϵ. Results indicate that for the supercritical Rayleigh numbers, the pulsation ω_c and ω_m have opposite signs. It means that the thermoconvective rolls advocated by the mean flow

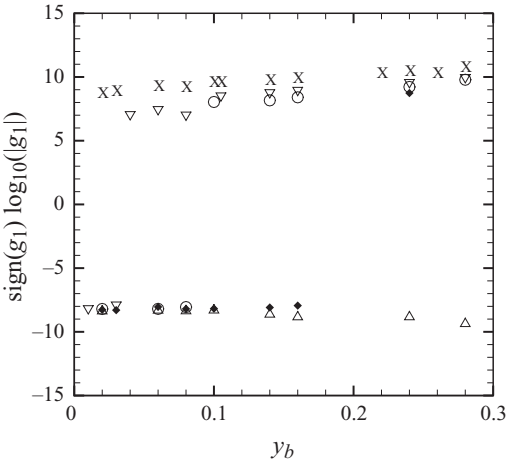

FIGURE 14. Evolution of g_1 as a function of y_b for different values of the Péclet number ($Pr = 50$). Triangles, $Pe = 2.5$; dark diamonds, $Pe = 1.5$; circles, $Pe = 1.25$; nabla symbols, $Pe = 1$; crosses, $Pe = 0.5$.

have decreasing phase velocity for increasing ϵ values. This result is in agreement with the effect of the mode 0 velocity which tends to slow down the mean flow. Moreover, for fixed values of ϵ, one observes that the nonlinear pulsation is stronger for weak values of y_b since the absolute values of ω_m decrease with the Bingham number.

Numerical results show that the value taken by g_1 is sensitive to the Reynolds and Prandtl values. Indeed, for increasing Reynolds number and fixed Prandtl number, g_1 decreases and reaches negative values. In other words, there exists a Reynolds number from which the bifurcation becomes subcritical. Moreover, when the Prandtl number varies between 1 and 100, one observes that the nature of the bifurcation changes around $Pe = Re\,Pr \simeq O(1)$. This unit Péclet value corresponds to the situation where there is an equilibrium between the convective (via inertia) and the diffusion effects. The bifurcation is found to be subcritical for $Pe > O(1)$, as is indicated in figure 14, which occurs when the convective effects are dominant. One can notice that the transition from supercritical to subcritical bifurcation occurs first for weak values of the yield stress.

Considering the different coefficients in (3.74), the numerical results show that the origin of the change in the nature of the bifurcation is mainly due to (i) the additional coefficient λ_{NH} given by (3.76) and (ii) the nonlinear Bingham coefficients, i.e. the quadratic $\mathscr{N}_{2B}$ and cubic $\mathscr{N}_3$ coefficients defined as follows:

$$\mathscr{N}_{2B} = \frac{1}{\langle \mathscr{D}.\boldsymbol{V}_1 E^1, \boldsymbol{V}_{adj}\rangle}\langle [N_2(\boldsymbol{V}_{-1}E^{-1}, \boldsymbol{V}_2 E^2)]_B, \boldsymbol{V}_{adj}\rangle, \tag{4.6}$$

$$\mathscr{N}_3 = \frac{1}{\langle \mathscr{D}.\boldsymbol{V}_1 E^1, \boldsymbol{V}_{adj}\rangle}\langle [N_3(\boldsymbol{V}_1 E^1,\ \boldsymbol{V}_1 E^1,\ \boldsymbol{V}_{-1}E^{-1})], \boldsymbol{V}_{adj}\rangle. \tag{4.7}$$

One notices that the dominant Bingham quadratic coefficient $\mathscr{N}_{2B}$ comes from the interaction between modes 2 and -1. The interaction between modes 1 and 0 is found to be negligible in the coefficient $\mathscr{N}_2$. The cubic coefficient $\mathscr{N}_3$ is only due to the effective viscosity perturbation and then is a factor of B.

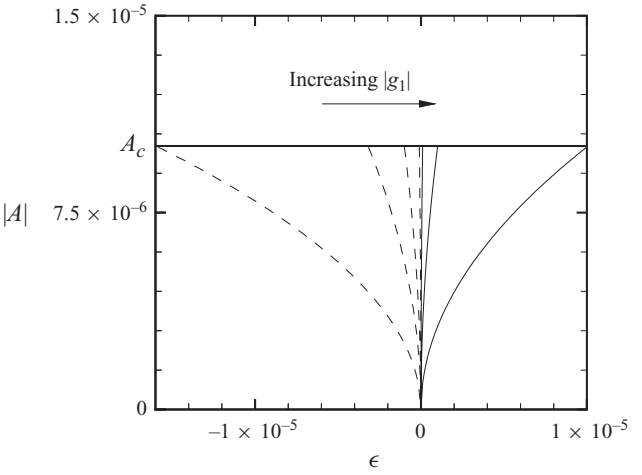

FIGURE 15. Schematic representation of the amplitude evolution as a function of ϵ for different values of g_1: – – –, subcritical bifurcation ($g_1 < 0$); ———, supercritical bifurcation ($g_1 > 0$).

For the range of tested values, the numerical results indicate that the sign of λ_{NH} and $\mathscr{N}_{2B}$ values is negative while the sign of $\mathscr{N}_3$ is positive. One observes that for $Pe = O(10^{-1})$, the dominant coefficient is $\mathscr{N}_3$, implying a supercritical bifurcation. Close to the value $Pe_c = O(1)$ and for weak values of y_b ($y_b < O(10^{-1})$), the coefficient λ_{NH} is the dominant contribution, which favours a subcritical bifurcation. This contribution is the consequence of the presence of the two phases 'solid' and 'liquid' via the yield surface conditions where $\dot{\gamma} = 0$.

For increasing y_b values ($y_b > O(10^{-1})$), the sign of g_1 is mainly determined by the contribution (ii) via the balance between $\mathscr{N}_{2B}$ and $\mathscr{N}_3$ values, which have opposite signs. Then, for $y_b > O(10^{-1})$ and close to $Pe_c = O(1)$, results can be summarized as follows.

(i) $Pe < Pe_c$ (dominant diffusion effects): $|\mathscr{N}_{2B}| < \mathscr{N}_3$ then $g_1 > 0$ and the bifurcation is supercritical.

(ii) $Pe > Pe_c$ (dominant convective effects): $|\mathscr{N}_{2B}| > \mathscr{N}_3$ then $g_1 < 0$ and the bifurcation is subcritical.

Finally, for weak values of y_b, the change in the nature of the bifurcation is mainly due to the yield surface conditions $\dot{\gamma} = 0$ via the additional coefficient λ_{NH}. For $y_b > O(10^{-1})$, the subcritical bifurcation is mainly due to the variations of the effective viscosity through the quadratic Bingham coefficient.

Furthermore, numerical results indicate that the change of the g_1 sign occurs for a very weak variation of the Péclet number, i.e. $\Delta Pe = O(10^{-3})$. In this respect, the transition from a supercritical to a subcritical bifurcation would be difficult to observe. On the other hand, the perturbed modes vary weakly with Pe meaning that the restrictive condition (4.1) imposed on the amplitude $|A|$ remains constant by varying weakly the Péclet number. Considering a supercritical bifurcation, the maximal value of $|A|$ corresponds to the saturated amplitude A_c see (4.3). One notices that the amplitude remains weak if ϵ values are also weak. For the range of values considered in the study, for weak y_b, one finds that $|A| < O(10^{-5})$, then $\epsilon < O(10^{-4})$. This range of values leads to fluctuations of the Rayleigh numbers of the order $O(10)$. It means that the problem rapidly becomes nonlinear, in terms of increasing

Ra values. In the Newtonian case, the validity domain of this analysis is larger and the numerical results of g_1 lead to finite and limited values ($g_1 \sim O(10)$). In this sense, the perturbation amplitudes reach values which can be experimentally observed and compared with the weakly nonlinear analysis (Ouazzani *et al.* 1994).

5. Conclusion

In this paper, we have investigated the yield stress effect on the nonlinear features of the RBP flow above criticality. A weakly nonlinear analysis based on the amplitude expansion is used in this study. Although Squire's theorem does not apply to our problem, the study was restricted to the two-dimensional case.

The mathematical formulation is presented and solutions are determined numerically by means of a fourth-order-centred finite-difference scheme. Compared with the Newtonian case, two phases, solid-like and liquid-like, have to be considered and additional nonlinear terms appear in the momentum equations via the viscosity perturbation. This study presents the influence of the yield stress and the shear-thinning behaviour on the determination of the quadratic modes and the perturbation amplitude evolution. In particular, we show that the nonlinear stability of the Bingham RBP flow is quite different from the Newtonian case, even at the limit $y_b \to 0$ since a thin unyielded region separates the two yielded regions. The determination of the quadratic modes, particularly mode 0, permits one to highlight the effect of the shear-thinning behaviour via the viscosity variations in the yielded regions. The increase in the degree of the nonlinearity of the rheological behaviour intensifies the mode 0.

The determination of the amplitude equation permits one to shed light on an abrupt change in the bifurcation nature at $Pe_c \approx O(1)$, critical value which depends on y_b. Indeed, we show that for weak values of the Péclet number ($Pe \leqslant Pe_c$) the bifurcation is supercritical while above Pe_c the bifurcation becomes subcritical. An interesting influence has also been underlined in our study: it concerns the presence of the plug regions, which involves specific (inhomogeneous) conditions at yield surfaces. These non-homogeneous boundary conditions at the yield surfaces tend to promote a subcritical bifurcation since their contribution to g_1 is dominant for weak thickness of the plug zone. For $y_b > O(10^{-1})$, the subcritical bifurcation is mainly due to the variations of the effective viscosity through the quadratic Bingham coefficient. It highlights the dominant effect of the shear-thinning behaviour, when $y_b > O(10^{-1})$, on the nature of the bifurcation, which is confirmed by the results given in the Rayleigh–Bénard configuration, by Khayat (1996), considering the Carreau–Yasuda model, and the one given by Cheng & Lai (2008), considering viscoplastic fluids, in fully yielded configuration. In these papers, the authors highlight clearly a transition from a supercritical bifurcation to a subcritical one, increasing the shear-thinning behaviour.

The range of the weakly nonlinear validity has also been discussed. One finds that the range of validity is very narrow, regarding the amplitude values. Indeed, in order to keep the fundamental mode as the dominant perturbation mode, a restricted condition is given on the amplitude value. Numerical results indicate that the framework of this stability analysis corresponds, as it is assumed, to small-amplitude perturbation, i.e. $|A| < O(10^{-5})$. In addition, this study shows that this condition is satisfied if ϵ, the reduced control parameter, also remains small ($\epsilon < O(10^{-4})$), meaning that the perturbed flow rapidly becomes fully nonlinear above criticality. The small perturbation assumes implicitly that the topology of

the perturbed flow is unchanged compared with the base flow (similar to the linear-stability assumptions). It means that, in the framework of the weakly nonlinear analysis, the central unyielded region is weakly perturbed, and the flow remains divided into two separate yielded and unyielded regions. Outside this framework, the question is when the unyielded zone would break up due to the onset and the evolution of the thermoconvective rolls. One aspect of our study would be to carry on the (weakly) nonlinear analysis, increasing the number of perturbation modes. In the Bingham case, this can be developed until the plug zone breaks up, and consists in considering a larger number of perturbation modes. It could provide interesting information on (i) the evolution of the finite amplitude perturbation and (ii) the condition above which the plug would break. This constitutes one aspect of our work.

The knowledge of the flow features above the break-up of the unyielded region is still a tedious problem. The difficulty is due to the fact that the stress is indeterminate in unyielded regions, considering the constitutive Bingham law (or the generalized Herschel–Bulkley law). In general, the Bingham (or Herschel–Bulkley) model is frequently used since it describes laminar flows well. However, considering the situations where the topology is modified and is not known *a priori*, these models are not adapted for theory. Several issues can be considered in order to overlap this limiting case: (i) perform experiments or direct numerical simulations by means of the augmented Lagrangian algorithm from Fortin & Glowinski (1983), which is widely used (e.g. Huilgol & Panizza 1995; Vinay, Wachs & Agassant 2005; Zhang, Vola & Frigaard 2006), (ii) consider a more realistic model which describes a yielded gel, with an elastic behaviour for instance. These issues constitute other aspects of our work.

Appendix A. Yield surface conditions

A.1. *The yield condition*

At the yield surfaces ($y = y_i^{\pm}$), the yield condition is $\dot{\gamma}(\boldsymbol{U}_b + \boldsymbol{u})|_{y_i^{\pm}} = 0$.

The Taylor expansion of each rate of strain components is given in the following.

(i) $\dot{\gamma}_{xx}|_{y_i^{\pm}} = 0 \Leftrightarrow \left.\dfrac{\partial u}{\partial x}\right|_{y_i^{\pm}} = 0$, leading to

$$\left.\frac{\partial u}{\partial x}\right|_{y_i^{\pm}} = \left.\frac{\partial u}{\partial x}\right|_{\pm y_b} + \left(\pm Y^{\pm}\right)\left[\frac{\partial^2 u}{\partial x \partial y}\right]_{\pm y_b} + \frac{\left(\pm Y^{\pm}\right)^2}{2}\left[\frac{\partial^3 u}{\partial x \partial y \partial y}\right]_{\pm y_b} + \cdots . \tag{A 1}$$

(ii) $\dot{\gamma}_{yy}|_{y_i^{\pm}} = 0 \Leftrightarrow \left.\dfrac{\partial v}{\partial y}\right|_{y_i^{\pm}} = 0$:

$$\left.\frac{\partial v}{\partial y}\right|_{y_i^{\pm}} = \left.\frac{\partial v}{\partial y}\right|_{\pm y_b} + \left(\pm Y^{\pm}\right)\left[\frac{\partial^2 v}{(\partial y)^2}\right]_{\pm y_b} + \frac{\left(\pm Y^{\pm}\right)^2}{2}\left[\frac{\partial^3 v}{(\partial y)^3}\right]_{\pm y_b} + \cdots . \tag{A 2}$$

(iii) $\dot{\gamma}_{xy}|_{y_i^{\pm}} = 0 \Leftrightarrow \left[\frac{\partial(U_b+u)}{\partial y} + \frac{\partial v}{\partial x}\right]_{y_i^{\pm}} = 0$:

$$\left[\frac{\partial(U_b+u)}{\partial y} + \frac{\partial v}{\partial x}\right]_{y_i^{\pm}} = \left.\frac{\partial U_b}{\partial y}\right|_{\pm y_b} + \left[(\pm Y^{\pm})\left[\frac{\partial^2 U_b}{(\partial y)^2}\right]_{\pm y_b} + \left.\frac{\partial u}{\partial y}\right|_{\pm y_b} + \left.\frac{\partial v}{\partial x}\right|_{\pm y_b}\right]$$
$$+ \left[(\pm Y^{\pm})\left[\frac{\partial^2 u}{(\partial y)^2} + \frac{\partial^2 v}{\partial x \partial y}\right]_{\pm y_b}\right] + \left[\frac{(\pm Y^{\pm})^2}{2}\left[\frac{\partial^3 u}{(\partial y)^3}\right]_{\pm y_b}\right.$$
$$\left. + \frac{(\pm Y^{\pm})^2}{2}\left[\frac{\partial^3 v}{\partial x \partial y^2}\right]_{\pm y_b}\right] + \cdots . \tag{A 3}$$

A.2. *Velocity continuity*

The velocity in the unyielded region is deduced considering the translational motion of this zone which implies that $\partial \boldsymbol{U}/\partial x = \partial \boldsymbol{U}/\partial y = \boldsymbol{0}$. In particular, at the yield surfaces, one can write:

$$\left.\frac{\partial u}{\partial x}\right|_{y_i^{\pm}} = \dot{\gamma}_{xx}|_{y_i^{\pm}} = 0, \tag{A 4}$$

$$\left.\frac{\partial v}{\partial y}\right|_{y_i^{\pm}} = \dot{\gamma}_{yy}|_{y_i^{\pm}} = 0, \tag{A 5}$$

$$\left.\frac{\partial(U_b+u)}{\partial y}\right|_{y_i^{\pm}} = \left.\frac{\partial v}{\partial x}\right|_{y_i^{\pm}} = 0. \tag{A 6}$$

Equations (A 4) and (A 7) have already been considered with (A 1) and (A 2). Expanding (A 6), one can obtain

$$\left.\frac{\partial U_b}{\partial y}\right|_{\pm y_b} + (\pm Y^{\pm})\left[\frac{\partial^2 U_b}{(\partial y)^2}\right]_{\pm y_b} + \left.\frac{\partial u}{\partial y}\right|_{\pm y_b} + (\pm Y^{\pm})\left[\frac{\partial^2 u}{(\partial y)^2}\right]_{\pm y_b}$$
$$+ \frac{(\pm Y^{\pm})^2}{2}\left[\frac{\partial^3 u}{(\partial y)^3}\right]_{\pm y_b} + \cdots = 0 \tag{A 7}$$

and

$$\left.\frac{\partial v}{\partial x}\right|_{\pm y_b} + (\pm Y^{\pm})\left[\frac{\partial^2 v}{\partial x \partial y}\right]_{\pm y_b} + \frac{(\pm Y^{\pm})^2}{2}\left[\frac{\partial^3 v}{\partial x \partial y^2}\right]_{\pm y_b} + \cdots = 0. \tag{A 8}$$

Finally, (A 1), (A 2), (A 7) and (A 8) correspond to the conditions at the yield surfaces. Considering the perturbation solution (3.33), each mode condition is obtained by identifying the order of amplitude perturbation. They are given in the following subsections.

A.3. *Linear mode yield surface conditions*

The linear mode is given in terms of velocity and yield surface positions by $\left[(u_1, v_1), \pm Y_1^{\pm}\right]$. The conditions at the yield surfaces $y = y_i^{\pm}$ are given by

$$\left.\frac{\partial u_1}{\partial x}\right|_{\pm y_b} = 0, \tag{A 9}$$

$$\left.\frac{\partial v_1}{\partial y}\right|_{\pm y_b} = 0, \tag{A 10}$$

$$\pm Y_1^{\pm} D^2 U_b(\pm y_b) + \left.\frac{\partial u_1}{\partial y}\right|_{\pm y_b} = 0, \tag{A 11}$$

$$\left.\frac{\partial v_1}{\partial x}\right|_{\pm y_b} = 0. \tag{A 12}$$

Similar conditions can be written for the complex conjugate $[(u_{-1}, v_{-1}), \pm Y_{-1}^{\pm}]$.

A.4. *Quadratic modes yield surface conditions*

(i) Mode 0: $[(u_0(y), 0), \pm Y_0^{\pm}]$

$$\left.\frac{\partial u_0}{\partial y}\right|_{\pm y_b} \pm Y_0^{\pm} D^2 U_b(\pm y_b) \pm Y_1^{\pm} \left.\frac{\partial^2 u_{-1}}{\partial y^2}\right|_{\pm y_b} \pm Y_{-1}^{\pm} \left.\frac{\partial^2 u_1}{\partial y^2}\right|_{\pm y_b} = 0. \tag{A 13}$$

(ii) Mode 2: $[A^2((u_2, v_2), \pm Y_2^{\pm})]$

$$\left.\frac{\partial u_2}{\partial x}\right|_{\pm y_b} \pm Y_1^{\pm} \left.\frac{\partial^2 u_1}{\partial x \partial y}\right|_{\pm y_b} = 0, \tag{A 14}$$

$$\left.\frac{\partial v_2}{\partial y}\right|_{\pm y_b} \pm Y_1^{\pm} \left.\frac{\partial^2 v_1}{\partial y^2}\right|_{\pm y_b} = 0, \tag{A 15}$$

$$\left.\frac{\partial u_2}{\partial y}\right|_{\pm y_b} \pm Y_2^{\pm} D^2 U_b(\pm y_b) \pm Y_1^{\pm} \left.\frac{\partial^2 u_1}{\partial y^2}\right|_{\pm y_b} = 0, \tag{A 16}$$

$$\left.\frac{\partial v_2}{\partial x}\right|_{\pm y_b} \pm Y_1^{\pm} \left.\frac{\partial^2 v_1}{\partial x \partial y}\right|_{\pm y_b} = 0. \tag{A 17}$$

Appendix B. Nonlinear expression of the stress tensor: the Bingham RBP case

B.1. *Stress tensor*

Considering the particular Bingham RBP case, one can simplify (3.16)–(3.18) as follows. First, the expression of the stress tensor associated to the basic flow is

$$\boldsymbol{\tau}_b = \begin{pmatrix} \tau_{bxx} & \tau_{bxy} \\ \tau_{bxy} & \tau_{byy} \end{pmatrix} = \begin{pmatrix} 0 & \dfrac{(DU_b)(B + \dot{\gamma}_b)}{\dot{\gamma}_b} \\ \dfrac{(DU_b)(B + \dot{\gamma}_b)}{\dot{\gamma}_b} & 0 \end{pmatrix}. \tag{B 1}$$

Concerning the perturbed flow, we obtain for the linear term

$$\boldsymbol{\tau}_1 = \begin{pmatrix} 2\left(1 + \dfrac{B}{\dot{\gamma}_b}\right)\partial_{xy}\psi & \partial_{yy}\psi - \partial_{xx}\psi \\ \partial_{yy}\psi - \partial_{xx}\psi & -2\left(1 + \dfrac{B}{\dot{\gamma}_b}\right)\partial_{xy}\psi \end{pmatrix} \tag{B 2}$$

and for the quadratic nonlinear term

$$\boldsymbol{\tau}_2 = \frac{1}{Pr\ Re}\begin{pmatrix} \dfrac{-2B\,\partial_{xy}\psi\,(\partial_{yy}\psi - \partial_{xx}\psi)}{DU_b\,\dot{\gamma}_b} & \dfrac{-B\,(\partial_{xy}\psi)^2}{2\,DU_b\,\dot{\gamma}_b} \\ \dfrac{-B\,(\partial_{xy}\psi)^2}{2\,DU_b\,\dot{\gamma}_b} & \dfrac{2B\,\partial_{xy}\psi\,(\partial_{yy}\psi - \partial_{xx}\psi)}{DU_b\,\dot{\gamma}_b} \end{pmatrix}. \tag{B 3}$$

Finally, the cubic term of the tensor is

$$\boldsymbol{\tau}_3 = \begin{pmatrix} \tau_{3xx} & \tau_{3xy} \\ \tau_{3xy} & \tau_{3yy} \end{pmatrix}, \tag{B 4}$$

with

$$\tau_{3xx} = -\tau_{3yy} = \frac{-B\,\partial_{xy}\psi\,(-2\,(\partial_{yy}\psi)^2 + (\partial_{xy}\psi)^2 + 4\,(\partial_{yy}\psi)(\partial_{xx}\psi) - 2\,(\partial_{xx}\psi)^2)}{(Pr\ Re)^2\ \dot{\gamma}_b^3} \tag{B 5}$$

and

$$\tau_{3xy} = \frac{B(\partial_{xy}\psi)^2\,(\partial_{yy}\psi - \partial_{xx}\psi)}{2\,\dot{\gamma}_b^3 (Pr\,Re)^2}. \tag{B 6}$$

B.2. *Quadratic and cubic terms of the vorticity equation*

For readability reasons, the following expressions are given in terms of velocity (defined in (2.1*b*)).

Developing the quadratic part of the vorticity equation (defined in (3.26)) using expressions (B 3)–(B 6) of the stress tensor perturbation, one obtains

$$\begin{aligned}(Pr\ Re)N_{21} = {} & Re(-u\,\Delta v + v\,\Delta u) + B\left[4\partial_{xy}\left(\frac{\partial_x u(\partial_y u + \partial_x v)}{(DU_b)^2}\right)\right] \\ & + B\left[\frac{1}{2}\,\mathrm{sign}(DU_b)\left(D^2 - \partial_x^2\right) \circ \left(\frac{\partial_x u}{DU_b}\right)^2\right]\end{aligned} \tag{B 7}$$

and

$$\begin{aligned}(Pr\ Re)^2\,N_{31} = {} & 2\,B\,D\left[\frac{1}{\dot{\gamma}_b^3}\partial_x((\partial_x u)^3 - 2\,\partial_x u(\partial_x v + \partial_y u)^2)\right] \\ & - B\,D^2\left[\frac{1}{\dot{\gamma}_b^3}(\partial_x u)^2(\partial_y u + \partial_x v)\right] + \frac{B}{\dot{\gamma}_b^3}\partial_{xx}((\partial_x u)^2(\partial_y u + \partial_x v)).\end{aligned} \tag{B 8}$$

Appendix C. Calculations of mode 0 boundary conditions

The additional boundary conditions of mode 0 are obtained writing the momentum equilibrium of an element of the perturbed plug zone as displayed in figure 16. In this respect, we define the domain $\Omega_s = [d - X\,; d + X] \times [-y_i\,; y_i]$, with d being a constant. The momentum equilibrium is given by

$$\frac{\mathrm{d}}{\mathrm{d}t}\int\int\int_{\Omega_s} \boldsymbol{u}_i\,\mathrm{d}\mathscr{V} = \oint_{\delta\Omega_s} \sigma_{ij}(\boldsymbol{U}_b + \boldsymbol{u})\,n_j\,\mathrm{d}S + \int\int\int_{\Omega_s} Ra\,(T_b + \theta)\,\delta_{i2}\,e_2\,\mathrm{d}\mathscr{V}. \tag{C 1}$$

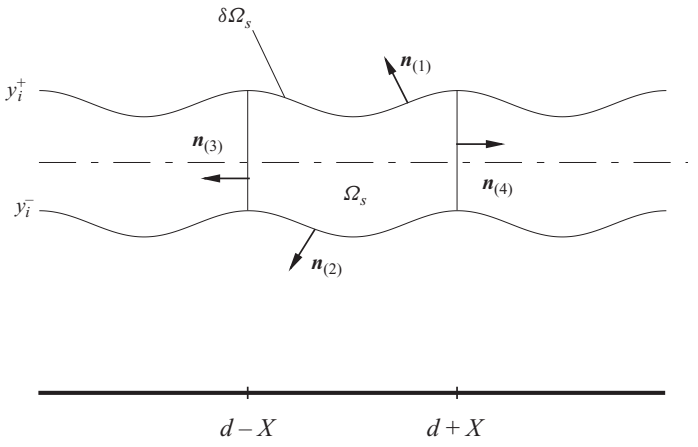

FIGURE 16. Scheme of the perturbed unyielded region.

The normal vectors associated to faces (1), (2), (3) and (4) can be, respectively, written to quadratic order:

$$\boldsymbol{n}_{(1)} = \frac{1}{\sqrt{1+(\partial_x Y^+)^2}} \begin{pmatrix} \partial_x Y^+ \\ 1 \end{pmatrix} = \begin{pmatrix} \partial_x Y^+ + \cdots \\ 1 - 1/2(\partial_x Y^+)^2 + \cdots \end{pmatrix}, \tag{C 2}$$

$$\boldsymbol{n}_{(2)} = \begin{pmatrix} -\partial_x Y^- + \cdots \\ -1 + 1/2(\partial_x Y^-)^2 + \cdots \end{pmatrix}, \tag{C 3}$$

$$\boldsymbol{n}_{(3)} = \begin{pmatrix} 1 \\ 0 \end{pmatrix}, \quad \boldsymbol{n}_{(4)} = \begin{pmatrix} -1 \\ 0 \end{pmatrix}. \tag{C 4}$$

We know that the velocities $\boldsymbol{u}_1$ and $\boldsymbol{u}_2$ vanish in the unyielded region (defined in (3.36) and (3.45)). Considering (3.33), we know that '$E^0\,\boldsymbol{u}_0$' does not depend on time t. Furthermore, the quasi-stationary assumption on the amplitude permits cancellation of the first term in (C 1). Finally the equilibrium can be written as follows:

$$\oint_{\delta\Omega_s} \sigma_{ij}(\boldsymbol{U}_b + \boldsymbol{u})\, e_j \,\mathrm{d}S + \int\int\int_{\Omega_s} Ra(T_b + \theta)\delta_{i2}\, e_2 \,\mathrm{d}\mathscr{V} = 0. \tag{C 5}$$

Expanding this equation we obtain

$$\begin{aligned} &\int_{d-X}^{d+X} [\partial_x Y^{\pm} \times ((-p_b - p)\,\delta_{i1} + \tau_{i1}(\boldsymbol{U}_b + \boldsymbol{u}))]_{-y_i}^{y_i} \mathrm{d}x \\ &\quad + \int_{d-X}^{d+X} \left[(1 - 1/2(\partial_x Y^{\pm})^2) \times (-(p_b + p)\,\delta_{i2} + \tau_{i2}(\boldsymbol{U}_b + \boldsymbol{u}))\right]_{-y_i}^{y_i} \mathrm{d}x \\ &\quad + \int_{-y_i}^{y_i} [-p_b\,\delta_{i1} + \tau_{i1}(\boldsymbol{U}_b + \boldsymbol{u})]_{d-X}^{d+X} \,\mathrm{d}y + \int_{-y_i}^{y_i}\int_{-X}^{X} Ra(T_b + \theta)\delta_{i2} \,\mathrm{d}x\,\mathrm{d}y = 0. \end{aligned} \tag{C 6}$$

Since the required condition corresponds to the mode 0 identification, we can notice that the functions to integrate do not depend on x except p_b, the pressure of the basic flow as given by (2.5).

Let us define P_b as follows:

$$P_b = p_b - P_{md} - p_{ref}, \tag{C 7}$$

with P_{md} the mean pressure in the interval $[d - X; d + X]$. Since P_{md} and p_{ref} are constant values, the integral of p_b is equal to the integral of P_b. Moreover, one can notice that in the case $d = 0$, $P_b = p_b - p_{ref}$ since $P_{m0} = 0$. Then one can write:

$$\int_{-y_i}^{y_i}\int_{d-X}^{d+X} p_b e_j \,\mathrm{d}S = \int_{-y_i}^{y_i}\int_{-X}^{X} P_b\, e_j \,\mathrm{d}S \tag{C 8}$$

$$= \int_{-y_i}^{y_i}\int_{-X}^{X}\left(-Ra\,\frac{y^2}{2} - \frac{B}{y_b}x\right) e_j \,\mathrm{d}S. \tag{C 9}$$

C.1. *The x-projection: case* $i = 1$

The projection of (C 6) along x can be written as follows:

$$\int_{-X}^{X} B_1 \,\mathrm{d}x + \int_{-X}^{X} B_2 \,\mathrm{d}x + \int_{-y_i}^{y_i} B_3 \,\mathrm{d}y = 0 \tag{C 10}$$

with

$$B_1 = [\partial_x Y^{\pm} \times (-P_b - p + \tau_{xx}(\Psi))]_{-y_i}^{y_i}, \tag{C 11}$$

$$B_2 = \left[\left(1 - 1/2(\partial_x Y^{\pm})^2\right) \times \tau_{xy}(\Psi)\right]_{-y_i}^{y_i} \tag{C 12}$$

and

$$B_3 = \int_{-y_i}^{y_i} [-P_b + \tau_{xx}\,(\Psi)]_{-X}^{X} \,\mathrm{d}y. \tag{C 13}$$

In the following sections, we propose to identify mode 0 of the terms B_1, B_2 and B_3.

C.1.1. $\mathscr{M}_0(B_1)$ *calculation*

Considering (3.33), one has

$$\mathscr{M}_0(B_1) = [\partial_x Y_1^{\pm} \times \mathscr{M}_{-1}(-P - p + \tau_{xx}(\Psi))]_{-y_i}^{y_i} + [\partial_x Y_{-1}^{\pm} \times \mathscr{M}_1(-P - p + \tau_{xx}(\Psi))]_{-y_i}^{y_i}. \tag{C 14}$$

The Taylor expansion around y_b permits one to write

$$\mathscr{M}_1\left([-P - p + \tau_{xx}(\Psi)]_{-y_i}^{y_i}\right) = [\pm Y_1^{\pm} Ra\; y]_{-y_b}^{y_b} - [p_1]_{-y_b}^{y_b} + [\tau_{1xx}(\psi_1)]_{-y_b}^{y_b}, \tag{C 15}$$

$$\mathscr{M}_{-1}\left([-P - p + \tau_{xx}(\Psi)]_{-y_i}^{y_i}\right) = [\pm Y_{-1}^{\pm} Ra\; y]_{-y_b}^{y_b} - [p_{-1}]_{-y_b}^{y_b} + [\tau_{1xx}(\psi_{-1})]_{-y_b}^{y_b}, \tag{C 16}$$

with

$$\tau_{1xx}(\psi_{\pm 1}) = 2\left(1 + \frac{B}{\dot{\gamma}_b}\right) \times (\pm \mathrm{i}\alpha\, Df_{\pm 1}). \tag{C 17}$$

One knows that

$$\lim_{y \to \pm y_b} \frac{Df_1}{\dot{\gamma}_b} = \lim_{\pm y_b} \frac{D^2 f_1}{D\dot{\gamma}_b} = \frac{\pm Y_1^{+}\, D^2 U_b(\pm y_b)}{\mp D^2 U_b(\pm y_b)} = -Y_1^{\pm} \quad \text{and} \quad \lim_{y \to \pm y_b} \frac{Df_{-1}}{\dot{\gamma}_b} = -Y_{-1}^{\pm}, \tag{C 18}$$

and using the boundary conditions (3.40), one can obtain

$$[\tau_{1xx}(\psi_{\pm 1})]_{-y_b}^{y_b} = \mp 2\mathrm{i}\alpha\, B\, Y_{\pm 1}^{+} \pm 2\mathrm{i}\alpha\, B\, Y_{\pm 1}^{-}. \tag{C 19}$$

Moreover, concerning the pressure terms, writing the x-component of the Navier–Stokes equation at $y = y_b$ and using the pressure continuity at this point, we obtain

$$p_{\pm1}(y_b) = \pm\frac{2\,B\,\alpha}{\mathrm{i}}Y^+_{\pm1} \pm \frac{1}{\mathrm{i}\alpha}D^3 f_{\pm1}(y_b), \quad \text{and} \quad p_{\pm1}(-y_b) = \pm\frac{2\,B\,\alpha}{\mathrm{i}}Y^-_{\pm1} \pm \frac{1}{\mathrm{i}\alpha}D^3 f_{\pm1}(-y_b). \tag{C 20}$$

Finally, the identification of B_1 to order $|A|^2$ is given by

$$\mathscr{M}_0(B_1) = Y_1^+ D^3 f_{-1}(y_b) - Y_1^- D^3 f_{-1}(-y_b) + Y_{-1}^+ D^3 f_1(y_b) - Y_{-1}^- D^3 f_1(-y_b). \tag{C 21}$$

C.1.2. *$\mathscr{M}_0(B_2)$ calculation*

$$B_2 = \left(1 - 1/2(\partial_x Y^\pm)^2\right) \times [\tau_{xy}(\Psi)]^{y_i}_{-y_i}. \tag{C 22}$$

The Taylor expansion around y_b of the different terms can be written as follows:

$$\tau_{xy}(\Psi)|_{y_i} = \tau_{xy}(\Psi)|_{y_b} + Y^+[\partial_y \tau_{xy}(\Psi)]_{y_b} + \frac{(Y^+)^2}{2}[\partial_{yy}\tau_{xy}(\Psi)]_{y_b} + \cdots. \tag{C 23}$$

The same expansions are written around $y = -y_b$.

After some algebra, one obtains

$$\begin{aligned}\mathscr{M}_0(B_2) = [Du_0]^{y_b}_{-y_b} - \frac{B}{y_b}(Y_0^+ + Y_0^-) + B\,\alpha^2(|Y_1^-|^2 + |Y_1^+|^2) + Y_1^+ D^3 f_{-1}(y_b) \\ + Y_1^- D^3 f_{-1}(-y_b) + Y_{-1}^+ D^3 f_1(y_b) + Y_{-1}^- D^3 f_1(-y_b).\end{aligned} \tag{C 24}$$

C.1.3. *$\mathscr{M}_0(B_3)$ calculation*

$$\mathscr{M}_0\left(\int_{-y_i}^{y_i} B_3\,\mathrm{d}y\right) = \mathscr{M}_0\left(\int_{-y_i}^{y_i} [-P]^X_{-X}\,\mathrm{d}y\right), \tag{C 25}$$

$$= \left(Y_0^+ + Y_0^-\right) \times 2X\,\frac{8\,Re\,Pr}{(1-y_b)^2}, \tag{C 26}$$

$$= \left(Y_0^+ + Y_0^-\right) \times 2X\,\frac{B}{y_b}. \tag{C 27}$$

C.1.4. *Conclusion: the momentum equation along x*

Equation (C 10) written in terms of mode 0 leads finally to

$$[Du_0]^{y_b}_{-y_b} = -\alpha^2\,B(|Y_1^+|^2 + |Y_1^-|^2) - 2(Y_1^+ D^3 f_{-1}(y_b) + Y_{-1}^+ D^3 f_1(y_b)). \tag{C 28}$$

C.2. *The y-projection: case $i = 2$*

The projection of (C 6) along y can be written as follows:

$$\int_{-X}^{X} C_1\,\mathrm{d}x + \int_{-X}^{X} [C_2 + C_3 + C_4]\,\mathrm{d}x + \int_{-y_i}^{y_i} C_5\,\mathrm{d}y + C_6 = 0 \tag{C 29}$$

with

$$C_1 = [\partial_x Y^\pm \times \tau_{xy}(\Psi)]^{y_i}_{-y_i}, \qquad C_2 = \left[\left(1 - 1/2(\partial_x Y^\pm)^2\right) \times \tau_{yy}(\Psi)\right]^{y_i}_{-y_i}, \tag{C 30}$$

$$C_3 = [-(P+p)]^{y_i}_{-y_i}, \qquad C_4 = \left[-1/2(\partial_x Y^\pm)^2 \times (-P-p)\right]^{y_i}_{-y_i}, \tag{C 31}$$

$$C_5 = [\tau_{xy}(\Psi)]^X_{-X} \quad \text{and} \quad C_6 = Ra\int_{-y_i}^{y_i}\int_{-X}^{X}(T_b + \theta)\,\mathrm{d}x\,\mathrm{d}y. \tag{C 32}$$

C.2.1. $\mathscr{M}_0(C_1)$ *calculation*

As for the previously discussed methods, we use the Taylor expansion and then we identify the terms of the order $|A|^2$:

$$\begin{aligned}\mathscr{M}_0\big([\partial_x Y^+ \times \tau_{xy}(\Psi)]_{y_i}\big) &= \mathrm{i}\alpha\big([Y_1^+\,\tau_{1xy}(\psi_{-1})]_{y_b} - [Y_{-1}^+\,\tau_{1xy}(\psi_1)]_{y_b}\big)\\ &\quad + \mathrm{i}\alpha\big([Y_{-1}^+ Y_1^+ \partial_y \tau_{bxy}]_{y_b} - [Y_1^+ Y_{-1}^+ \partial_y \tau_{bxy}]_{y_b}\big)\\ &= \mathrm{i}\alpha\big([Y_1^+ \tau_{1xy}(\psi_{-1})]_{y_b} - [Y_{-1}^+ \tau_{1xy}(\psi_1)]_{y_b}\big). \qquad \text{(C 33)}\end{aligned}$$

A similar expression is developed at $y = -y_i$.

Evaluating the stresses, one finally obtains

$$\begin{aligned}\mathscr{M}_0(C_1) &= \mathrm{i}\alpha(Y_1^+ D^2 f_{-1}(y_b) - Y_{-1}^+ D^2 f_1(y_b))\\ &\quad - \mathrm{i}\alpha(Y_1^- D^2 f_{-1}(-y_b) - Y_{-1}^- D^2 f_1(-y_b)). \qquad \text{(C 34)}\end{aligned}$$

C.2.2. $\mathscr{M}_0(C_2)$ *calculation*

Since $\tau_{byy} = 0$, then $\mathscr{M}_0(C_2) = \mathscr{M}_0([\tau_{yy}(\Psi)]_{-y_i}^{y_i})$.

The Taylor expansion permits one to write as follows:

$$\begin{aligned}\mathscr{M}_0(C_2) &= [Y_1^+ \partial_y \tau_{1yy}(\psi_{-1})]_{y_b} + [Y_{-1}^+ \partial_y \tau_{1yy}(\psi_1)]_{y_b}\\ &\quad + [Y_1^- \partial_y \tau_{1yy}(\psi_{-1})]_{-y_b} + [Y_{-1}^- \partial_y \tau_{1yy}(\psi_1)]_{-y_b}. \qquad \text{(C 35)}\end{aligned}$$

C.2.3. $\mathscr{M}_0(C_3)$ *calculation*

$$\mathscr{M}_0(C_3) = \mathscr{M}_0\big([-P]_{-y_i}^{y_i}\big) - \mathscr{M}_0\big([p]_{-y_i}^{y_i}\big), \qquad \text{(C 36)}$$

with

$$\mathscr{M}_0\big([-P]_{-y_i}^{y_i}\big) = Ra\; y_b\big(Y_0^+ - Y_0^-\big) + Ra\big(|Y_1^+|^2 - |Y_1^-|^2\big), \qquad \text{(C 37)}$$

and using the Taylor expansions:

$$\mathscr{M}_0\big([-p]_{-y_i}^{y_i}\big) = [-p_0]_{-y_b}^{y_b} - Y_1^+ \partial_y p_{-1}\big|_{y_b} - Y_{-1}^+ \partial_y p_1\big|_{y_b} - Y_1^- \partial_y p_{-1}|_{-y_b} - Y_{-1}^- \partial_y p_1|_{-y_b}. \qquad \text{(C 38)}$$

For the term p_0, one can write the Navier–Stokes equation along y, identified in terms of mode 0: one obtains

$$\begin{aligned}0 &= -\partial_y p_0 + \partial_x \tau_{1xy}(u_0) + \partial_y \tau_{1yy}(u_0) + Ra\,\theta_0 + \partial_y(\tau_{2yy}(\psi_1, \psi_{-1})\\ &\quad + \tau_{2yy}(\psi_{-1}, \psi_1)) + \partial_x(\tau_{2xy}(\psi_1, \psi_{-1}) + \tau_{2xy}(\psi_{-1}, \psi_1)), \qquad \text{(C 39)}\end{aligned}$$

with

$$\partial_x \tau_{1xy}(u_0) = 0,\ \partial_y \tau_{1yy}(u_0) = 0 \quad \text{and} \quad \partial_x(\tau_{2xy}(\psi_1, \psi_{-1}) + \tau_{2xy}(\psi_{-1}, \psi_1)) = 0.$$

Integrating this equation, one obtains

$$\begin{aligned}[p_0]_{-y_b}^{y_b} &= \lim_{y_b}[\tau_{2yy}(\psi_1, \psi_{-1}) + \tau_{2yy}(\psi_{-1}, \psi_1)]\\ &\quad - \lim_{-y_b}[\tau_{2yy}(\psi_1, \psi_{-1}) + \tau_{2yy}(\psi_{-1}, \psi_1)] + \int_{-y_b}^{y_b} Ra\; T_0\,\mathrm{d}y, \qquad \text{(C 40)}\end{aligned}$$

with

$$\lim_{y_b}[\tau_{2yy}(\psi_1,\psi_{-1})+\tau_{2yy}(\psi_{-1},\psi_1)] = 2\mathrm{i}\alpha B\left[D^2f_{-1}(y_b)\lim_{y_b}\frac{Df_1}{\dot\gamma_b}-D^2f_1(y_b)\lim_{y_b}\frac{Df_{-1}}{\dot\gamma_b}\right] = 0, \tag{C 41}$$

and similarly

$$\lim_{-y_b}[\tau_{2yy}(\psi_1,\psi_{-1})+\tau_{2yy}(\psi_{-1},\psi_1)] = 0. \tag{C 42}$$

We finally obtain

$$\mathscr{M}_0(C_3) = Ra\left[y_b\left(Y_0^+-Y_0^-\right)+\left(|Y_1^+|^2-|Y_1^-|^2\right)-\int_{-y_b}^{y_b}T_0\,\mathrm{d}y\right]-Y_1^+\partial_y p_{-1}\big|_{y_b} - Y_{-1}^+\partial_y p_1\big|_{y_b}-Y_1^-\partial_y p_{-1}|_{-y_b}-Y_{-1}^-\partial_y p_1|_{-y_b}. \tag{C 43}$$

Remark. The terms involving $\partial_y p_{\pm1}$ are not evaluated at this stage, since they could be combined with the stress terms of (C 35) writing the Navier–Stokes equation.

C.2.4. $\mathscr{M}_0(C_4)$ *calculation*

$$\mathscr{M}_0(C_4) = \mathscr{M}_0\left(\left[-1/2(\partial_x Y^{\pm})^2\times(-P)\right]_{-y_i}^{y_i}\right) = \left(-Ra\,\frac{y_b^2}{2}-\frac{B}{y_b}\mathscr{M}_0(x)\right)\left(\alpha^2|Y_1^+|^2-\alpha^2|Y_1^-|^2\right). \tag{C 44}$$

Developing the function $x\mapsto x$, defined on $[-X;X]$, in the base $(e^{\mathrm{i}n\alpha x})_n$ as follows:

$$x = a_0+\sum_n a_n\cos(n\alpha x)+\mathrm{i}\sum_n b_n\sin(n\alpha x). \tag{C 45}$$

One obtains

$$a_0=0;\quad \forall n\in\mathbb{N}^*\quad a_n=0\quad\text{and}\quad b_n=-\frac{\mathrm{i}}{n\alpha}. \tag{C 46}$$

Then

$$x=\sum_n\frac{1}{n\alpha}\sin(n\alpha x) \tag{C 47}$$

and

$$\mathscr{M}_0(x)=a_0=0. \tag{C 48}$$

Finally, one can write

$$\mathscr{M}_0(C_4) = -\alpha^2\,Ra\,\frac{y_b^2}{2}\left(|Y_1^+|^2-|Y_1^-|^2\right). \tag{C 49}$$

C.2.5. $\mathscr{M}_0(C_5)$ *calculation*

$$[\tau_{xy}(\Psi)]_{-X}^X = [\tau_{bxy}(\Psi)]_{-X}^X+[\tau_{1xy}(u_0)]_{-X}^X+[\tau_{1xy}(\psi_1)]_{-X}^X+[\tau_{1xy}(\psi_{-1})+\cdots]_{-X}^X, \tag{C 50}$$

$$[\tau_{bxy}(\Psi)]_{-X}^X = [\tau_{1xy}(u_0)]_{-X}^X = 0, \tag{C 51}$$

since $\tau_{bxy}(\Psi)$ and $\tau_{1xy}(u_0)$ do not depend on x. The remaining terms are periodic with period $2X$; then

$$C_5 = 0. \tag{C 52}$$

C.2.6. *$\mathscr{M}_0(C_6)$ calculation*

$$C_6 = Ra \int_{-y_i}^{y_i} \int_{-X}^{X} (T_b + \theta_0)\, \mathrm{d}x\, \mathrm{d}y, \tag{C 53}$$

since $\int_{-X}^{X} T_1\, \mathrm{d}x = \int_{-X}^{X} T_{-1}\, \mathrm{d}x = \int_{-X}^{X} T_2\, \mathrm{d}x = \int_{-X}^{X} T_{-2}\, \mathrm{d}x = 0$. One can write

$$C_6 = 2X\, Ra \left(\left[-\frac{y^2}{2} \right]_{-y_i}^{y_i} + \int_{-y_i}^{y_i} \theta_0\, \mathrm{d}y \right), \tag{C 54}$$

$$\mathscr{M}_0(C_6) = 2X Ra \left(-\left(|Y_1^+|^2 - |Y_1^-|^2 \right) + \mathscr{M}_0 \left(\int_{-y_i}^{y_i} \theta_0\, \mathrm{d}y \right) \right). \tag{C 55}$$

Introducing Θ_0, a primitive of θ_0, and using a Taylor expansion of Θ_0 around $\pm y_b$, we can show that

$$\mathscr{M}_0 \left(\int_{-y_i}^{y_i} \theta_0\, \mathrm{d}y \right) = \int_{-y_b}^{y_b} \theta_0\, \mathrm{d}y. \tag{C 56}$$

Further,

$$\mathscr{M}_0(C6) = 2X\, Ra \left(-|Y_1^+|^2 + |Y_1^-|^2 + \int_{-y_b}^{y_b} \theta_0\, \mathrm{d}y \right). \tag{C 57}$$

C.2.7. *Conclusion: the momentum equation along y*

In conclusion, the momentum conservation along y can be written as follows:

$$\begin{aligned} Ra\, y_b \left(Y_0^+ - Y_0^- \right) = Ra \left(Y_1^+ \theta_{-1}(y_b) + Y_{-1}^+ \theta_1(y_b) + Y_1^- \theta_{-1}(-y_b) + Y_{-1}^- \theta_1(-y_b) \right) \\ + Ra \frac{y_b^2}{2} \alpha_c^2 \left(|Y_1^+|^2 - |Y_1^-|^2 \right). \end{aligned} \tag{C 58}$$

Appendix D. Adjoint operator

The determination of the adjoint problem consists in seeking operators $\mathscr{D}^\dagger$, $\mathscr{L}_R^\dagger$ such that

$$\langle \mathscr{D}\, \boldsymbol{V},\, \boldsymbol{V}_{adj} \rangle = \langle \boldsymbol{V},\, \mathscr{D}^\dagger\, \boldsymbol{V}_{adj} \rangle \qquad \text{and} \qquad \langle \mathscr{L}_R\, \boldsymbol{V},\, \boldsymbol{V}_{adj} \rangle = \langle \boldsymbol{V},\, \mathscr{L}_R^\dagger\, \boldsymbol{V}_{adj} \rangle, \tag{D 1}$$

where $\boldsymbol{V}_{adj} = (f_{adj}, \theta_{adj})^T$ corresponds to the adjoint vector and the Hermitian scalar product is defined by

$$\langle \boldsymbol{V}, \boldsymbol{W} \rangle = \int \frac{1}{\mathscr{V}}\, \boldsymbol{V} \cdot \boldsymbol{W}^*\, \mathrm{d}\Omega, \tag{D 2}$$

with $\mathscr{V}$ the volume of the domain Ω and W^* the complex conjugate of W.

Finally, the adjoint problem is given as follows. In the yielded region:

$$\mathrm{i}\alpha\, c \begin{pmatrix} \mathscr{D}_1^\dagger & 0 \\ 0 & -1 \end{pmatrix} \begin{pmatrix} f_{adj} \\ \theta_{adj} \end{pmatrix} = \begin{pmatrix} \mathscr{L}_{R1}^\dagger & -\mathrm{i}\alpha \\ \mathrm{i}\alpha\, Ra & \mathscr{L}_{R4}^\dagger \end{pmatrix} \begin{pmatrix} f_{adj} \\ \theta_{adj} \end{pmatrix}$$

with $\mathscr{L}_{R1}^\dagger$, $\mathscr{L}_{R3}^\dagger$ and $\mathscr{D}_1^\dagger$ given by

$$\begin{cases} \mathscr{L}_{R1}^\dagger \equiv -\mathrm{i}\alpha Re \left[U_b \left(D^2 - \alpha^2 \right) + 2DU_b\, D \right] - \left(D^2 - \alpha^2 \right)^2 + 4\alpha^2\, BD \left(\dfrac{D}{|DU_b|} \right), \\ \mathscr{L}_{R4}^\dagger \equiv -\mathrm{i}\alpha\, Pr\, Re\, U_b - (D^2 - \alpha^2), \\ \mathscr{D}_1^\dagger \equiv \mathscr{D}_1. \end{cases}$$

In the unyielded region:

$$f_{adj} = 0,$$
$$\mathscr{L}_{R3}\,\theta_{adj} = c\,\theta_{adj}.$$

Boundary conditions for $\boldsymbol{V}_{adj}$ are similar to those given for the linear mode $\boldsymbol{V}_1$, i.e. (3.38)–(3.40).

REFERENCES

Albaalbaki, B. & Khayat, R. E. 2008 Finite-amplitude Rayleigh–Bénard convection for weakly shear thinning fluids. *J. Phys.: Conf. Ser.* **137**, 012024.

Ashrafi, N. & Khayat, R. E. 1999 Shear-thinning-induced chaos in Taylor–Couette flow. *Phys. Rev.* E **61** (2), 1455–1567.

Balmforth, N. & Rust, A. 2009 Weakly nonlinear viscoplastic convection. *J. Non-Newton. Fluid Mech.* **158** (1–3), 36–45.

Bingham, E. C. 1922 *Fluidity and Plasticity*. McGraw-Hill.

Carrière, P. & Monkewitz, P. 2001 Transverse-roll global modes in a Rayleigh–Bénard–Poiseuille system with streamwise variable heating. *Eur. J. Mech.* B *Fluids* **20**, 751–770.

Cheng, P. J. & Lai, H. Y. 2008 Finite-amplitude long-wave instability of Bingham liquid films. *Nonlinear Anal.: Real World Appl.* **10**, 1500–1513.

Fortin, M. & Glowinski, R. 1983 *The Augmented Lagrangian Method*. Elsevier.

Fujimura, K. 1989 The equivalence between two perturbation methods in weakly nonlinear stability theory for parallel shear flows. *Proc. R. Soc. Lond. Ser.* A **424**, 373–392.

Fujimura, K. 1997 Center manifold reduction and the Stuart–Landau equation for fluid motions. *Proc. R. Soc. Lond. Ser.* A **453**, 181–203.

Gage, K. S. & Reid, W. H. 1968 The stability of thermally stratified plane Poiseuille flow. *J. Fluid Mech.* **33**, 21–32.

Generalis, S. C. & Fujimura, K. 2009 The range of validity of weakly nonlinear theory in the Rayleigh–Bénard problem. *J. Phys. Soc. Japan* **78** (8), 084401.

Georgievskii, D. V. 1993 Stability of two and three dimensional viscoplastic flows and generalized Squire theorem. *Isv. AN SSSR Mekh. Tverdogo Tela.* **28**, 117–123.

Gross, L. K. 2002 Weakly non-linear dynamics of interface propagation. *Stud. Appl. Math.* **108**, 323–350.

Herbert, T. 1980 Nonlinear stability of parallel flows by high-order amplitude expansions. *AIAA J.* **18** (3), 243–248.

Herbert, T. 1983 On perturbation methods in nonlinear stability theory. *J. Fluid Mech.* **126**, 167–186.

Huilgol, R. R. & Panizza, M. P. 1995 On the determination of the plug flow region in Bingham fluids through the application of variational inequalities. *J. Non-Newton. Fluids Mech.* **58**, 207–217.

Khayat, R. E. 1996 Chaos in thermal convection of weakly shear-thinning fluids. *J. Non-Newton. Fluid Mech.* **63**, 153–178.

Kuo, H. L. 1996 Solution of the nonlinear equations of cellular convection and heat transport. *J. Fluid Mech.* **10**, 611–634.

Malkus, W. V. R. & Veronis, G. 1958 Finite amplitude cellular convection. *J. Fluid Mech.* **4**, 225–260.

Martinand, D., Carrière, P. & Monkewitz, P. 2006 Three-dimensional global instability modes associated with a localized hot spot in Rayleigh–Bénard–Poiseuille convection. *J. Fluid Mech.* **551**, 275–301.

Métivier, C., Frigaard, I. A. & Nouar, C. 2009 Non-linear stability of the Bingham–Rayleigh–Bénard Poiseuille flow. *J. Non-Newton. Fluid Mech.* **158**, 127–131.

Métivier, C. & Nouar, C. 2008 On linear stability of Rayleigh–Bénard Poiseuille flow of viscoplastic fluids. *Phys. Fluids* **20** (10), 104106.1–104106.7.

Métivier, C., Nouar, C. & Brancher, J. P. 2005 Linear stability involving the Bingham model when the yield stress approaches zero. *Phys. Fluids* **17** (10), 104101.1–104101.14.

Müller, H. W., Lücke, M. & Kamps, M. 1989 Convective patterns in horizontal flow. *Europhys. Lett*. **10** (5), 451.

Nicolas, X. 2002 Revue bibliographique sur les écoulements de Poiseuille–Rayleigh–Bénard: écoulements de convection mixte en conduites rectangulaires horizontales chauffées par le bas. *Intl J. Therm. Sci*. **41**, 961–1016.

Oldroyd, J. G. 1947*a* Two-dimensional plastic flow of a Bingham solid. *Proc. Camb. Phil. Soc*. **43**, 383–395.

Oldroyd, J. G. 1947*b* A rational formulation of the equations of plastic flow for a Bingham solid. *Proc. Camb. Phil. Soc*. **43**, 100–105.

Ouazzani, M. T., Platten, J. K., Müller, H. W. & Lücke, M. 1994 Etude de la convection mixte entre deux plans horizontaux à températures différentes III. *Intl J. Heat Mass Transfer* **38** (5), 875–886.

Platten, J. K. 1971 A variational formulation for the stability of flows with temperature gradients. *Intl Engng Sci*. **9**, 855–869.

Reynolds, W. C. & Potter, M. C. 1967 Finite-amplitude instability of parallel shear flows. *J. Fluid Mech*. **27**, 465–492.

Schmid, P. J. & Henningson Dan, S. 2001 *Stability and Transition in Shear Flows*. Springer.

Vinay, G., Wachs, A. & Agassant, J. F. 2005 Numerical simulation of non-isothermal viscoplastic waxy crude oil flows. *J. Non-Newton. Fluid Mech*. **128**, 144–162.

Zhang, J., Vola, D. & Frigaard, I. A. 2006 Yield stress effects on Rayleigh–Bénard convection. *J. Fluid Mech*. **566**, 389–419.